Geochimica et Cosmochimica Acta 342 (2023) 31–44

Contents lists available at ScienceDirect

Geochimica et Cosmochimica Acta

journal homepage: www.elsevier.com/locate/gca

Chromium stable isotope distributions in the southwest Pacific Ocean and constraints on hydrothermal input from the Kermadec Arc

David J Janssen [a,b,*], Delphine Gilliard [a,c], Jörg Rickli [d], Philipp Nasemann [a], Andrea Koschinsky [e,f], Christel S Hassler [c,g], Andrew R Bowie [h], Michael J Ellwood [i], Charlotte Kleint [e,f], Samuel L Jaccard [a,c]

[a] Institute of Geological Sciences & Oeschger Centre for Climate Change Research, University of Bern, Baltzerstrasse 1-3, 3012 Bern, Switzerland
[b] Eawag – Swiss Federal Institute of Aquatic Sciences and Technology, Department Surface Waters, Seestrasse 79, 6047 Kastanienbaum, Switzerland
[c] Institute of Earth Sciences, University of Lausanne, Lausanne, Switzerland
[d] Institute of Geochemistry and Petrology, ETH Zürich, Zürich, Switzerland
[e] Department of Physics and Earth Sciences, Jacobs University Bremen, 28759 Bremen, Germany
[f] Center for Marine Environmental Sciences (MARUM), University of Bremen, 28359 Bremen, Germany
[g] Department F.-A. Forel for Environmental and Aquatic Sciences, University of Geneva, Uni Carl Vogt, 66 Bvd. Carl-Vogt, 1211 Geneva 4, Switzerland
[h] Institute for Marine and Antarctic Studies, University of Tasmania, 20 Castray Esplanade, Battery Point, Tasmania 7004, Australia
[i] Research School of Earth Sciences, Australian National University, Canberra, Australia

ARTICLE INFO

Article history:
Received 9 March 2022
Accepted 8 December 2022
Available online 12 December 2022
Associate editor: Rachael James

Keywords:
Chromium
GEOTRACES
Chromium isotopes
Hydrothermal flux
Paleoproxy

ABSTRACT

Special attention has been given to chromium (Cr) as a paleoproxy tracing redox cycling throughout Earth's history, due to differences in the solubility of its primary redox species at Earth's surface (Cr(III) and Cr(VI)) and isotope fractionation associated with their interconversion. In turn, chromium's paleoproxy potential has motivated studies of the modern ocean to better understand which processes drive its cycling and to constrain their impact on the Cr isotope composition (δ^{53}Cr) of seawater. Here, we present total dissolved seawater Cr concentrations and δ^{53}Cr along the GEOTRACES GP13 section. This section is a zonal transect extending from Australia in the subtropical southwest Pacific Ocean. Surface signals of local biological Cr cycling are minimal, in agreement with distributions of dissolved major nutrients as well as biologically-controlled trace metals in this low productivity, oligotrophic environment. Depth profiles have Cr concentration minima in surface waters and maxima at depth, and are largely shaped by the advection of nutrient- and Cr-rich subsurface waters rather than vertically-driven processes. Samples close to the sediment–water interface indicate important benthic Cr fluxes across the section.

The GP13 transect crosses the hydrothermally-active Kermadec Arc. Hydrothermal fluids (consisting of <15% background seawater) were collected from three venting sites at the Brothers Volcano (along the Kermadec Arc). These fluids yielded near-crustal δ^{53}Cr values (−0.17 to +0.08‰) and elevated [Cr] (7.5–23 nmol kg^{-1}, hydrothermal endmember [Cr] ≈ 8–27 nmol kg^{-1}), indicating that the Kermadec Arc may be an isotopically light Cr source. Dissolved [Fe] enrichments have been reported previously in deep waters (~1600–3000 m) along the GP13 transect, east of the Kermadec Arc. These same waters show elevated [Cr] compared to Circumpolar Deep Water ([Cr] = 3.88 ± 0.11, δ^{53}Cr = 0.89 ± 0.08, n = 32), with an average [Cr] accumulation of 0.71 ± 0.11 nmol kg^{-1} (1 SD), and an estimated δ^{53}Cr of +0.46 ± 0.30‰ (2 SD, n = 9) for the accumulated Cr. Comparing high-temperature vent and neutrally buoyant plume data, hydrothermal-sourced Cr is likely negligable compared to Cr contributions from other processes (benthic fluxes, release from particles), and the advection of more Cr-rich Pacific Deep Water. It is unlikely that hydrothermal vents would be a major contributor within the regional or global biogeochemical Cr cycle, even if hydrothermal fluxes change by orders of magnitude, and therefore δ^{53}Cr trends in the paleorecord may be attributable, at least in part, to major changes in other controls on Cr (e.g. widespread anoxia).

* Corresponding author at: Eawag – Swiss Federal Institute of Aquatic Sciences and Technology, Department Surface Waters, Seestrasse 79, 6047 Kastanienbaum, Switzerland.

E-mail addresses: david.janssen@eawag.ch (D.J Janssen), delphine.gilliard@unil.ch (D. Gilliard), joerg.rickli@erdw.ethz.ch (J. Rickli), a.koschinsky@jacobs-university.de (A. Koschinsky), christelshassler@gmail.com (C.S Hassler), Andrew.Bowie@utas.edu.au (A.R Bowie), michael.ellwood@anu.edu.au (M.J Ellwood), c.kleint@jacobs-university.de (C. Kleint), Samuel.Jaccard@unil.ch (S.L Jaccard).

https://doi.org/10.1016/j.gca.2022.12.010
0016-7037/

1. Introduction

Oceanic dissolved Cr concentrations ([Cr]) show surface minima and enrichments at depth (e.g. Campbell & Yeats, 1981), corresponding to a nutrient-type distribution. Surface ocean depletion reflects biological control through removal in the surface ocean, export to depth with biogenic particles, and regeneration in deep waters (e.g. Jeandel & Minster, 1987; Semeniuk et al., 2016; Janssen et al., 2020). However, the vertical and spatial gradients in [Cr] remain small (Jeandel & Minster, 1987; Moos & Boyle, 2019; Janssen et al., 2021; Pöppelmeier et al., 2021) compared to other nutrient-type elements (e.g. P, N, Cd, Zn; cf. Horner et al., 2021). The muted nutrient-type distribution of Cr is likely influenced by the primary redox states of Cr in oxic waters – Cr(III) and Cr(VI) – and their contrasting reactivity. The main chemical species that drive interconversions between these two redox species are Mn oxides and H_2O_2 (Cr(III) oxidation; Pettine et al., 1991; Milletto et al., 2021) as well as Fe(II) and sulfide (Cr(VI) reduction; Pettine et al., 1998; Kim et al., 2001). In oxic waters, Cr redox speciation is dominated by Cr(VI), a soluble oxyanion that has a low affinity for particulate organic material and mineral surfaces (Wang et al., 1997; Semeniuk et al., 2016). In contrast, Cr(III), accounting for $\leq$15% of total [Cr] in oxic waters (e.g. Murray et al., 1983; Jeandel & Minster, 1987; Achterberg & van den Berg, 1997; Janssen et al., 2020), is poorly soluble and readily scavenged (Wang et al., 1997; Semeniuk et al., 2016). Slight [Cr(III)] maxima in surface waters (e.g. Achterberg & van den Berg, 1997; Janssen et al., 2020) are likely driven by biological or photochemical reactions, potentially through the generation of known Cr reductants such as Fe(II) (Kieber & Helz, 1992; Hug & Laubscher, 1997). In contrast to Cr redox speciation in oxic waters, Cr(III) may dominate in oxygen minimum zones (OMZs), and local [Cr] minima are observed in the water column or at the sediment–water interface due to Cr reduction and removal (e.g. Murray et al., 1983; Rue et al., 1997; Moos et al., 2020; Nasemann et al., 2020; Huang et al., 2021). Therefore OMZs and the adjacent suboxic and anoxic sediments may be globally important for Cr removal, despite their limited spatial extent (e.g. Reinhard et al., 2013; Wei et al., 2018).

While stable isotope fractionation associated with Cr oxidation shows mixed trends, with enrichments in heavy isotopes, light isotopes or no fractionation in oxidized Cr (e.g. Zink et al., 2010; Milletto et al., 2021), Cr reduction is consistently associated with the enrichment of light isotopes in the reduced phase (e.g. Wanner & Sonnenthal, 2013). Therefore, Cr reduction and removal can regulate distributions of both [Cr] and δ^{53}Cr in the ocean. Indeed, the first inter-basin δ^{53}Cr dataset showed a tight linear correlation between δ^{53}Cr and ln[Cr], indicating that Cr distributions appear to reflect closed-system Rayleigh fractionation process(es) with an isotope enrichment factor (ε) ≈ -0.7 (Scheiderich et al., 2015). Consequently, Scheiderich et al. (2015) proposed that the two primary processes regulating [Cr] – biologically-mediated Cr export in surface waters and Cr reduction and removal in OMZs – also control δ^{53}Cr. Subsequent δ^{53}Cr research has targeted these processes. Biologically-mediated Cr export from the surface ocean has been shown to explain surface [Cr] deficits quantitatively and proceed with a fractionation comparable to that of the global δ^{53}Cr–ln[Cr] array (Janssen et al., 2020). Likewise, the release of Cr from biogenic particles in the water column and from surface sediments also follows the global array (Janssen et al., 2021). Isotopically light Cr is removed in OMZs, both in the water column (Moos et al., 2020; Huang et al., 2021) and near the sediment–water interface (Moos et al., 2020; Nasemann et al., 2020). The apparent isotope fractionation associated with OMZ Cr reduction and removal may be influenced by the partial retention of isotopically light Cr(III) in the dissolved phase (Nasemann et al., 2020; Huang et al., 2021; Wang, 2021), though fractionation factors remain poorly constrained. In addition to OMZs and biological export acting to regulate Cr removal, water mass circulation and mixing are important in shaping Cr and δ^{53}Cr depth profiles and global distributions (e.g. Moos & Boyle, 2019; Rickli et al., 2019, Janssen et al., 2021; Pöppelmeier et al., 2021; see also review in Horner et al., 2021). Marine sediments may also act as sources of Cr to the deep waters (e.g. Jeandel & Minster, 1987; Bauer et al., 2019; Janssen et al., 2021; Pöppelmeier et al., 2021). Available pore and bottom water data indicate that benthic sources may be significant, at least locally if not globally, and that the benthic Cr flux may be isotopically heavier than lithogenic material and isotopically lighter than the water column (Janssen et al., 2021).

Isotopic fractionations associated with Cr redox transformations have also driven interest in δ^{53}Cr as a paleoredox proxy (e.g. Frei et al., 2009; Planavsky et al., 2014). Initial studies applied an interpretive framework where oceanic δ^{53}Cr was controlled by terrestrial weathering (e.g. Frei et al., 2009). While such a framework may accurately reflect the primary controls on δ^{53}Cr over certain major global changes throughout Earth's history (e.g. atmospheric oxygenation), subsequent oceanographic research has identified clear control of δ^{53}Cr by processes acting in the ocean. Furthermore, questions surrounding the integrity of a diverse range of potential δ^{53}Cr archives have arisen (e.g. due to fractionation during incorporation of Cr into sediment phases, post-depositional modification through exchange with pore waters or early diagenesis, and overprinting by modern weathering signals; Albut et al., 2018; Bauer et al., 2018; Remmelzwaal et al., 2019; Frank et al., 2020; Wang et al., 2021; Janssen et al., 2022). Therefore, additional research on processes controlling oceanic δ^{53}Cr and Cr sequestration into marine sediments, as well as on the fidelity of sediment records, is needed to improve δ^{53}Cr-based paleoreconstructions.

One such gap in understanding the modern biogeochemical Cr cycle relates to hydrothermal circulation. While changing contributions of hydrothermally-sourced Cr have been inferred from the paleorecord (Holmden et al., 2016; Bauer et al., 2021; Yobo et al., 2022), potential hydrothermal Cr sources remain unconstrained in the modern global Cr budget in terms of both fluxes and isotope composition. Indeed, it is even unclear whether hydrothermal cycling acts as a net Cr source or sink in the ocean. Hydrothermal fluids are enriched in many trace metals (e.g. Metz & Trefry, 2000), and therefore may also be Cr-rich. However, these fluids can also be enriched in Cr reductants (reduced S, Fe(II); e.g. Field & Sherrell, 2000; Sander & Koschinsky, 2011). Precipitation reactions upon mixing of vent fluids with seawater may result in the scavenging of Cr sourced from both waters. Dissolved Cr data are scarce near vent systems, and while high-temperature vent fluids may show Cr enrichments over seawater (Jeandel & Minster, 1984), observations from deep waters and box models suggest that the balance may tip toward net Cr removal (Jeandel & Minster, 1984; Jeandel & Minster, 1987). Similar conclusions were drawn based on the Cr content of near-vent particles (Trocine & Trefry, 1988; Rudnicki & Elderfield, 1993; Feely et al., 1994) and marine sediments (Bauer et al., 2019). In some studies, this removal is proposed to be a globally significant process, though it should be noted that some scavenged Cr may be remobilized in Mn oxide-rich sediments near vents (Jeandel & Minster, 1984; Bauer et al, 2019). In contrast to the interpretations of a net sink, Sander & Koschinsky (2000) proposed that vents may be a Cr source, with Cr(III) stabilized in plume samples through organic complexation. This study, however, reports similarly elevated and scattered [Cr(III)] and total dissolved [Cr] away from the hydrothermal plume. Therefore, the results are difficult to explain by known oceanographic processes and do not offer unequivocal support for hydrothermally sourced Cr. No hydrothermal δ^{53}Cr data are

available, though previous studies (e.g. Reinhard et al., 2013; Holmden et al., 2016; Bauer et al., 2019, 2021; Yobo et al., 2022) have assumed hydrothermally-sourced Cr is isotopically equivalent to the continental crust ($\delta^{53}Cr \approx -0.1‰$, Schoenberg et al., 2008).

Here we present seawater [Cr] and $\delta^{53}Cr$ from the southwest Pacific Ocean. The samples span across the hydrothermally-active Kermadec Arc, thereby identifying the arc's regional impact on seawater Cr. Samples collected from vents at the Brothers Volcano provide direct insight into vent Cr fluxes and isotope composition. Together the data provide initial constraints on the impact of hydrothermal processes on oceanic [Cr] and $\delta^{53}Cr$.

2. Study area

Sampling was conducted in the austral autumn of 2011 during Leg 1 of GEOTRACES section GP13, a predominantly zonal transect heading east from the Australian coast near 30° S (Fig. 1). This transect extended from the Tasman Sea, which lies between Australia and New Zealand, into the South Pacific Gyre.

2.1. Surface currents and biological productivity

The southward-flowing East Australian Current (EAC) is found near the Australian coast (e.g. Ganachaud et al., 2014) and is characterized by relatively Fe-rich, nutrient-poor waters (Ellwood et al., 2018). The anticyclonic South Pacific Gyre, with eastward flow at the latitude of the GP13 transect, drives surface water circulation away from the coastal EAC (e.g. Ganachaud et al., 2014; Chiswell et al., 2015). Surface waters of the Tasman Sea and the South Pacific Gyre are highly depleted in macronutrients. The phytoplankton community is dominated by prokaryotes (*Prochlorococcus* and *Synechococcus*), with higher biomass toward the western end of the transect and much lower biomass in the more oligotrophic eastern end of the transect (Cabanes et al., 2020). Chlorophyll distributions show a persistent deep (~100 m) maximum in the South Pacific Gyre (Kiefer et al., 1989; Halm et al., 2012; Mingot et al., 2014; Caffin et al., 2018; Ellwood et al., 2018), which is regularly below the mixed layer (Mingot et al., 2014) including during this study (Fig. 2, see also Ellwood et al., 2018).

2.2. Intermediate and deep waters

The primary subsurface water masses in the region are Antarctic Intermediate Water (AAIW), Circumpolar Deep Water (CDW) and Pacific Deep Water (PDW). AAIW enters the northern Tasman Sea through the subtropical South Pacific and flows southward along the Australian coast. This Tasman Sea AAIW, centered around 800 m (neutral density (γ^n) = 27.1), is characterized by higher salinity and temperature and lower O_2 than the relatively younger AAIW in the Southern Ocean and the central South Pacific (Bostock et al., 2013). Northward-advecting AAIW, sourced more directly from the Southern Ocean, mixes with this Tasman AAIW in the eastern Tasman Sea and east of New Zealand, resulting in AAIW more characteristic of Southern Ocean endmembers toward the eastern end of the transect (Bostock et al., 2013). Chromium concentrations in Southern Ocean AAIW fall generally within a narrow range ([Cr] = 3.62 ± 0.08 nmol kg^{-1}, n = 16 samples, 26.8 < γ^n < 27.4; Rickli et al., 2019; Janssen et al., 2021), and are similar to Tasman AAIW ([Cr] = 3.39 ± 0.13 nmol kg^{-1}, n = 6 samples, 26.8 < γ^n < 27.4; Janssen et al., 2021).

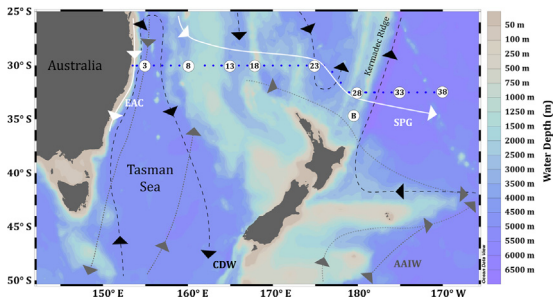

Fig. 1. Map of the GP13 transect. Stations on the GP13 Transect are shown as small blue circles, with large white circles (numbered) identifying stations sampled for Cr. The Brothers Volcano site (not a part of the GP13 Transect) is labelled as B. Bathymetry is shown on the color bar. Surface currents are shown as solid white lines with labels (EAC – East Australian Current), as well as the South Pacific Gyre (SPG). AAIW flow paths are shown as dotted grey lines, and CDW flow paths are shown as dashed black lines. Currents are adapted from Sokolov & Rintoul (2000), Bostock et al. (2013) and Ellwood et al. (2018).

CDW, composed of Upper and Lower components (UCDW and LCDW, respectively), is found below AAIW. UCDW, at γ^n < 28.0, is formed within the Antarctic Circumpolar Current (ACC) and is characterized by T > 1.5° C and salinity > 34.5. LCDW, at γ^n > 28.0, is colder, more saline, and more O_2-rich than UCDW (Orsi et al., 1995; Sloyan & Rintoul, 2001), and is formed south of the southern ACC boundary. CDW flows northward in the western Tasman Sea, but this source is kept to the western half of the basin at the latitude of the GP13 transect due to shallow topographic features (Fig. 1). The source of CDW to the rest of the GP13 transect (stations east of ~160° E) is from northward flow to the east of New Zealand, with southward flowing branches west of the Kermadec Ridge (~180°, see Section 2.3) (Sokolov & Rintoul, 2000). Chromium concentrations in UCDW and LCDW lie within a tight range in the Southern Ocean ([Cr] = 3.82 ± 0.07 nmol kg^{-1} (1SD, n = 20) and [Cr] = 3.97 ± 0.1 nmol kg^{-1} (1SD, n = 12) for UCDW and LCDW, respectively, Rickli et al., 2019; Janssen et al., 2021), indicating CDW sources to GP13 should have a relatively uniform Cr composition. Local topography restricted sampling to $\gamma^n \leq 28.2$, precluding strong influence of Antarctic Bottom Water (γ^n > 28.2, found below LCDW, Sloyan & Rintoul, 2001).

East of the Tasman Sea, deep waters along the GP13 transect are also impacted by older, southward-flowing PDW (Gebbie and Huybers, 2012; Zilberman et al., 2020). This PDW, found at similar densities as UCDW, is characterized by lower [O_2] (Sloyan & Rintoul, 2001), older radiocarbon ages (Gebbie and Huybers, 2012), and elevated macronutrients (e.g. Ellwood et al., 2018; George et al., 2019) compared to UCDW. PDW inflow extends from around 2000 to 4000 m, with a maximal southward flow centered around 3000 m depth (Zilberman et al., 2020). Chromium concentrations in PDW are variable (~4–5 nmol kg^{-1}, cf. Murray et al., 1983; Moos & Boyle, 2019; Janssen et al., 2021), and generally increase with water mass age (Janssen et al., 2021). However, no constraints on [Cr] in PDW near the GP13 transect are available.

2.3. Hydrothermal influence

The Kermadec Arc is a hydrothermally active system extending northward from New Zealand along the Kermadec Ridge. Multiple distinct submarine vent sites, at depths of the upper hundreds of meters to ~2000 m have been characterized along the ridge (e.g. de Ronde et al., 2001; Baker et al., 2003: de Ronde et al., 2007). The GP13 transect crosses the Kermadec Arc around 32.5° S and 180° (Station 28), where a plume of [Fe] has been observed extending eastward from the Kermadec Ridge (Ellwood et al., 2018). The deepest known hydrothermal sites located within ~150–320 km of the GP13 transect are Brothers, Healy, Harve and Rumble II W, (all ~1400–1700 m depth). These show enriched turbidity near their peaks, as well as their bases at 2000–3000 m (de Ronde et al., 2001; Baker et al., 2003: de Ronde et al., 2007).

Fluid chemistry is highly variable among specific volcano sites at the southern end of the Kermadec Arc (Kleint et al., 2019). At

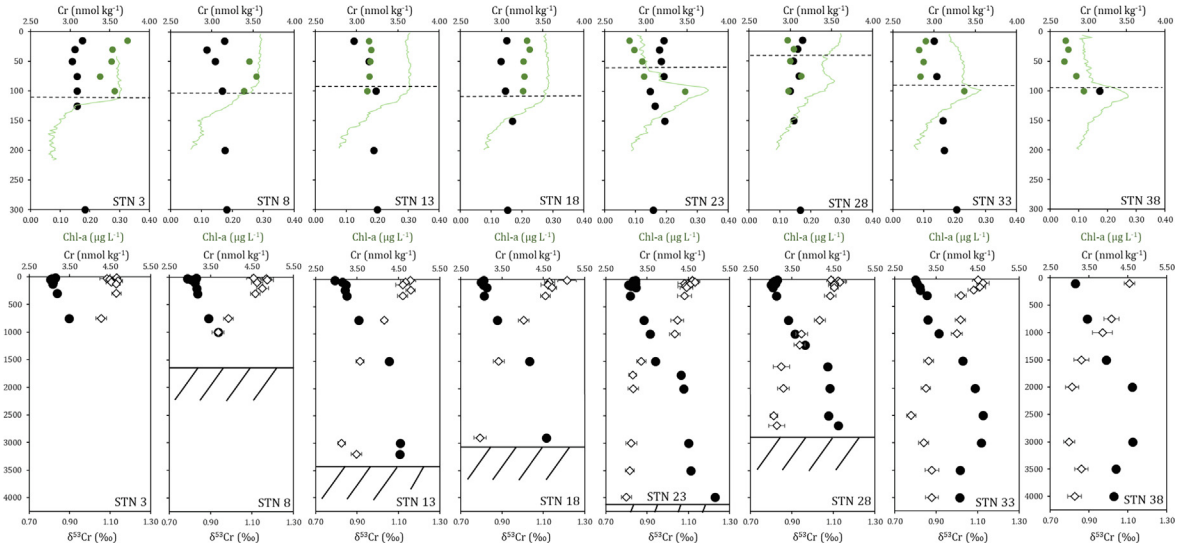

Fig. 2. Chromium concentration and δ^{53}Cr depth profiles. Concentrations are shown as circles, δ^{53}Cr as diamonds, chlorophyll-a concentrations from Cabanes et al. (2020) as green circles, and CTD chlorophyll fluorescence (unitless, scaling is consistent across plots) as light green lines. Dashed horizontal lines (upper panels) represent mixed layer depths and solid horizontal lines (lower panels) show sediment depth. Note the different [Cr] ranges for upper and lower panels.

the studied site closest to the GP13 transect, the Haungaroa Volcano (32.6° S, 179.6° E, ~680 m water depth), vent fluids are characterized by very low Fe/Mn, suggesting sub-seafloor removal of Fe through FeS precipitation (Kleint et al., 2019). However, this site is much shallower than the observed [Fe] plume along the GP13 transect and, given the high degree of heterogeneity along the southern Kermadec Arc, may differ chemically from the source of the [Fe] plume seen along GP13. While still considerably variable, high-temperature vent fluids from volcanoes at > 1000 m depth along the southern Kermadec Arc generally show [Fe] > [H_2S], and total dissolved Fe > [Fe(II)] (Kleint et al., 2019, 2022), with Fe(III) oxides important at some sites for metal transport within the plume (Kleint et al., 2022).

The Brothers Volcano site is composed of multiple distinct venting environments (de Ronde et al., 2001; Kleint et al., 2019, 2022; Neuholz et al., 2020). Samples presented here are from the northwest side of the caldera and the caldera upper wall, as well as the northward-propagating plume from this end of the caldera (Kleint et al., 2019, 2022; Neuholz et al., 2020). Vents at this site are characterized by high temperatures (~300 °C), low pH (pH ≈ 3) and high Fe:H_2S ratios (up to >10) (Kleint et al., 2019, 2022). The neutrally buoyant plume is diluted with ambient seawater > 10^2 times within days (Neuholz et al., 2020).

Southward-flowing PDW may also contain more distal sources of hydrothermally-derived metals from deep water (~2000–3000 m) venting sites along the East Pacific Rise (e.g. Fitzsimmons et al., 2014; Resing et al., 2015), consistent with Fe enrichments seen along the GP13 transect (Ellwood et al., 2018). Chromium may be stabilized and transported long distances by oxidation to Cr(VI), e.g. by Mn oxides (e.g. Milletto et al., 2021), and/or by complexation with organic ligands, known to stabilize many metals in hydrothermal plumes (e.g. Sander & Koschinsky, 2011).

3. Methods

3.1. Seawater sampling

Seawater samples (125 mL to 1 L) were collected on the *RV Southern Surveyor* in May to June 2011 during Leg 1 of the GEOTRACES GP13 section (Fig. 1). Sampling is described in detail in Cabanes et al. (2020) and Ellwood et al. (2018). In brief, samples were collected in Niskin-X bottles with a trace metal clean rosette system and gravity filtered through acid-cleaned 0.2 µm Acropak filters (Pall) into acid cleaned LDPE bottles under HEPA-filtered air in a clean container. The majority of the data reported here were obtained on seawater samples that were frozen upon collection and later thawed and acidified with 1 mL L^{-1} concentrated HCl (sub-boiling distilled). Acidified samples were stored at room temperature at least for 7 months before analysis. Additional samples (n = 20) were acidified upon collection with 1.2 mL L^{-1} 16 M HNO_3 and stored until analyzed (approximately 9.5 years). These samples are noted in the full data table (Table A.1), but show no difference from comparable frozen samples.

GP13 CTD data (temperature, salinity, chlorophyll fluorescence (uncorrected)), chlorophyll concentrations and macronutrient concentrations are available from the GEOTRACES Intermediate Data Product 2021 (GEOTRACES Intermediate Data Product Group, 2021) and/or have been published previously (e.g. Ellwood et al., 2018; Cabanes et al., 2020; George et al., 2019). The base of the mixed layer was defined as a change in γ^{η} of >0.03 kg m^{-3} compared to surface waters.

To better constrain hydrothermal endmember fluids, five additional samples are presented from the Brothers Volcano along the Kermadec Arc (e.g. de Ronde et al., 2001), collected on cruise SO253 onboard the *RV Sonne* from December 2016–January 2017. Three high-temperature fluids were collected from active vents by a remotely operated vehicle (ROV) using titanium syringe samplers. Two near-vent neutrally buoyant plume samples were collected by CTD-Rosette equipped with an in-situ turbidity sensor, with the plume identified in real time by sensors and Cr subsamples chosen based on this and trace metal data (Kleint et al., 2022). Samples were filtered through 0.2 µm polycarbonate filters and acidified to pH ≈ 2 with HCl (Suprapur, Merck). Any precipitates formed between sample collection and filtration would therefore be removed from the sample, and our data may reflect this. However, [Fe] compare well with samples from isobaric, gas tight samples (which preserve in situ pressure, see Kleint et al., 2019). Therefore we consider such phases to be minor. Sampling is described in more detail in Kleint et al. (2019, 2022).

3.2. Chromium concentration and stable isotope analyses

Chromium concentrations and stable isotope composition were analyzed at the University of Bern, Switzerland using procedures

described in Rickli et al. (2019), with modifications outlined in Janssen et al. (2020) and Nasemann et al. (2020). In brief, preliminary [Cr] was determined by isotope dilution on small subsamples (5–30 mL) on a Neptune Plus MC-ICP-MS (ThermoFisher) after Cr enrichment and purification by $Mg(OH)_2$ co-precipitation and cation exchange chromatography. These preliminary concentration data were used to determine appropriate double spike amounts for $\delta^{53}Cr$ analyses and are not presented here.

Chromium stable isotope compositions were determined on 125 mL to 1 L samples with a ^{50}Cr-^{54}Cr double spike. The seawater matrix was removed through Cr co-precipitation with $Mg(OH)_2$ by the addition of 5–9 mL 20–22% NH_3 (Romil UpA) per L seawater (Rickli et al., 2019; see also Moos & Boyle, 2019). This technique is known to capture both inorganic and organically complexed Cr (III) (Davidson et al., 2020), with all Cr present as Cr(III) after storage at low pH (Semeniuk et al., 2016). The precipitate was allowed to settle overnight and ~2/3 of the supernatant was carefully decanted prior to centrifugation and decanting of the reaming supernatant. The separated precipitate was dissolved in 2 M HCl and transferred to Teflon vials. Samples were dried and dissolved in 9 mL 0.022 M HCl in preparation for column chromatography. Chromium was purified by using a two step column chromatography procedure: (1) Anion exchange chromatography with AG1-X8 resin following Cr oxidation with 0.01 M $(NH_4)_2S_2O_8$ and reductive elution with 1 M HNO_3 + 2% H_2O_2 (Rickli et al., 2019; Janssen et al., 2020; Nasemann et al., 2020, see also Ball & Bassett, 2000); (2) cation exchange chromatography with AG 50 W-X8 resin (Rickli et al., 2019; see also Yamakawa et al., 2009). Chromium stable isotope composition was analyzed with a Neptune Plus MC-ICP-MS as described in Rickli et al. (2019), and data are reported relative to the reference material NIST SRM 979. Typical total yields for this procedure were around 50–70%, in agreement with other recent $\delta^{53}Cr$ studies employing $Mg(OH)_2$ co-precipitation (Moos & Boyle, 2019; Rickli et al., 2019). The five hydrothermal samples from the Brothers site were processed like normal seawater samples, though with smaller water volumes (15–125 mL) and lower [Mg] ([Mg] = 4.3 mM, or ~8% of normal seawater, for the sample with highest hydrothermal endmember contribution). For one high-temperature vent sample, replicate Cr enrichment was achieved by evaporation rather than co-precipitation, with a first purification step of Fe removal with anion exchange chromatography (e.g. Scheiderich et al., 2015) followed by the usual chromatographic procedures. This value agrees well with data obtained from co-precipitation (Table 2).

Precision was monitored with full replicates of OSIL seawater ($\delta^{53}Cr$ = +0.87 ± 0.02‰, 2 SD, n = 5), accuracy with repeated measurements of a Merck Cr(III) standard ($\delta^{53}Cr$ = −0.43 ± 0.03‰, 2 SD, n = 7; literature: $\delta^{53}Cr$ = −0.443 ± 0.022‰, 2 SD, Schoenberg et al., 2008). Internal uncertainties were typically 0.02–0.03‰ (2 SEM), except when only small sample volumes were available (<500 mL). External reproducibility for spiked NIST standards analyzed during the course of this study is 0.023‰ (2 SD, n = 68), applying a session-specific small correction (≤0.03 δ-units) based on the average NIST SRM 979 composition (e.g. Schoenberg et al., 2008). These session-specific corrections were also applied to the samples. External reproducibility for seawater replicates (500 mL to 1 L sample volume) based on our methodology has been determined to be 0.033‰ (2 SD) for $\delta^{53}Cr$ and 0.82% RSD for Cr (49 analyses of 17 samples, Janssen et al., 2020). Individual $\delta^{53}Cr$ data are shown with an external error of 0.033‰ or the internal uncertainty, whichever is larger, and 1% RSD for [Cr]. Natural variability for specific water masses and endmembers is reported based on the average and 2 SD for $\delta^{53}Cr$ and the average and 1 SD for [Cr].

4. Results

Chromium concentrations and $\delta^{53}Cr$ follow nutrient-type distributions, as observed throughout the global ocean (e.g. Campbell & Yeats, 1981; Murray et al., 1983; Jeandel & Minster, 1987; Moos & Boyle, 2019; Rickli et al., 2019; Janssen et al., 2020), with lowest [Cr] and highest $\delta^{53}Cr$ in surface waters, and with elevated [Cr] and lower $\delta^{53}Cr$ at depth (Figs. 2 and 3C, E). East-west gradients in [Cr] and $\delta^{53}Cr$ are minimal, mirroring macronutrient and hydrographic data (Fig. 3, Appendix Fig. 1). Within the surface mixed layer, dissolved [Cr] (~3 nmol kg^{-1}) and $\delta^{53}Cr$ (~1.1‰) are comparable to previous data from the open Pacific Ocean (Moos & Boyle, 2019; Janssen et al., 2020; Huang et al., 2021), while [Cr] is lower and $\delta^{53}Cr$ higher than reported for the Southern Ocean (Rickli et al., 2019). Chromium concentrations show minimal variability both along the transect and within the upper 200 m for each profile, below which a transition toward higher [Cr] and lower $\delta^{53}Cr$ begins (Figs. 2 and 3C, E). At 750–1000 m, the depth range where AAIW is centered, [Cr] corresponds to 3.50 ± 0.12 nmol kg^{-1} and $\delta^{53}Cr$ to 1.01 ± 0.07‰ (1 SD and 2 SD respectively, n = 12, station 38 1000 m not included – see section 5.3).

Below AAIW, [Cr] and $\delta^{53}Cr$ continue to increase and decrease, respectively. This reflects the dominance of U- and LCDW and PDW, which are further enriched in [Cr] and are isotopically light relative to AAIW (Rickli et al., 2019; Janssen et al., 2021). At stations 13–23, at depths ≥ 1500 m and >150 m above the seafloor, [Cr] is 4.33 ± 0.27 nmol kg^{-1} (1 SD) with a $\delta^{53}Cr$ of 0.86 ± 0.07‰ (2 SD) (n = 9, note that no deep water data are available at stations

Table 1
Calculated deep water Cr accumulation in samples potentially influenced by the Kermadec Arc.

Station	Depth m	$[Cr]_{accumulated}$ nmol kg^{-1}	$[Cr]_{accumulated}$ 1SD nmol kg^{-1}	$\delta^{53}Cr_{accumulated}$ ‰	$\delta^{53}Cr_{accumulated}$ 2SD ‰	Water Mass
28	1600	0.54	0.11	0.47	0.65	PDW/UCDW
28	2000	0.67	0.11	0.61	0.50	PDW/UCDW
28	2500	0.64	0.11	0.27	0.49	PDW/UCDW
28	2680	0.79	0.11	0.46	0.44	PDW/UCDW
33	2000	0.66	0.11	0.55	0.49	PDW/UCDW
33	2500	0.82	0.11	0.20	0.39	PDW/UCDW
33	3000	0.61	0.14	0.68	0.55	LCDW
38	2000	0.84	0.11	0.41	0.41	PDW/UCDW
38	3000	0.81	0.15	0.48	0.42	LCDW
Combined Estimate of Accumulated Cr		**Average $[Cr]_{accumulated}$**	**$[Cr]_{accumulated}$ 1SD**	**Average $\delta^{53}Cr_{accumulated}$**	**$\delta^{53}Cr_{accumulated}$ 2SD**	**N**
Stns 28–38, 1600–3000 m		nmol kg^{-1}	nmol kg^{-1}	‰	‰	
Accumulated Cr		0.71	0.11	+0.46	0.30	9

Accumulated Cr is calculated by mass balance relative to Southern Ocean endmembers. The results reflect contributions from mixing with PDW, Cr from sinking particles and/or benthic sources, as well as potential hydrothermal contributions (see Section 5.3.2). Uncertainties follow standard error propagation.

Table 2
Chromium composition of vent sites and neutrally buoyant plumes at the Brothers Volcano (Kermadec Arc).

Sample	Latitude	Longitude	Notes	Depth m	[Cr] nmol kg^{-1}	δ^{53}Cr ‰	2SEM ‰	Temp °C	pH	Eh mV	Sal	Mg mM	[H_2S] mM	[SO_4^{2-}]	[Fe^{2+}] mM	[Fe] mM	[Mn] mM	EM %
046_CTD-T_8	34.84917° S	179.05308° E	Cone plume	1278	4.01	0.90	0.05	–	–	–	–	–	–	–	–	81 × 10^{-6}	11 × 10^{-6}	–
046_CTD-T_6	34.84917° S	179.05308° E	Deep plume	1584	4.49	0.94	0.04	–	–	–	–	–	–	–	–	12 × 10^{-6}	31 × 10^{-6}	–
067_ROV_11F	34.85918° S	179.05229° E	Caldera wall & upper Caldera	1374	7.47[A]	–0.05[A]	0.08[A]	311	3.2	211	45.1	4.9	1.05	0.4	9.59	11.9	2.3	91
064_ROV_5F	34.86103° S	179.05766° E	Caldera wall & upper Caldera	1600	8.42	–0.07	0.10	170	3.5	133	43.1	4.3	–	2.0	5.37	8.2	0.6	92
081_ROV_3F	34.86128° S	179.05777° E	Caldera wall & upper Caldera	1619	23.30	0.04	0.04	305	3.5	153	43.0	8.2	–	3.4	6.45	7.6	0.6	85

Ancillary data (temperature, pH, Eh, salinity, Mg, H_2S, SO_4, metal concentrations & endmember percent estimated from [Mg], with background seawater [Mg] = 51 mM based on locally measured values) are from Kleint et al. (2019; 2022). For temperature, salinity, Fe^{2+} and H_2S these come from samples collected at the same depth and within 0.00005 decimal degrees of the Cr samples.
[A] Data represent a weighted mean of two independently prepared subsamples (separate spiking, chemistry and analysis; individual subsamples: ([Cr] = 7.33 nmol kg^{-1}, δ^{53}Cr = –0.02 ± 0.12‰ and [Cr] = 7.62 nmol kg^{-1}, δ^{53}Cr = –0.06 ± 0.10‰).

3 & 8, and stations 28–38 are discussed in Section 5.3). This is somewhat enriched in Cr relative to CDW in the Southern Ocean ([Cr] = 3.88 ± 0.11 nmol kg^{-1}, n = 32), though the two are isotopically indistinguishable (Southern Ocean CDW δ^{53}Cr = 0.89 ± 0.08‰, n = 32; Rickli et al., 2019; Janssen et al., 2021). High-temperature hydrothermal vent fluids from the Brothers Volcano (Kermadec Arc) have distinctly higher [Cr] (7.5 to 22.3 nmol kg^{-1}) and lower δ^{53}Cr (δ^{53}Cr = −0.07 ± 0.10‰ to +0.04 ± 0.04‰, 2SEM) relative to surrounding seawater, indicating that vents may be a local source of Cr. Potential hydrothermal signals are also seen in deep waters east of the Kermadec Arc, corresponding to depths where hydrothermally-sourced [Fe] has been observed previously (Ellwood et al., 2018). These samples show elevated [Cr] relative to CDW sources (Fig. 4), but within ranges reported previously in PDW in the North Pacific (Murray et al., 1983; Moos & Boyle, 2019; Janssen et al., 2021). Finally, local maxima are observed in the deepest samples, when these samples are within 150 m of the sediment–water interface (e.g. Stations 18–28 in Fig. 2).

5. Discussion

5.1. [Cr] and δ^{53}Cr in the upper 200 m

Chromium concentrations and stable isotope distributions show minimal variability in surface waters. Macronutrient concentrations (PO_4, NO_3, $Si(OH)_4$; Fig. 3; Ellwood et al., 2018; George et al., 2019) and nutrient-type trace metals (e.g. Cd, George et al., 2019) also show relatively uniform concentrations in the upper few hundred meters along the transect, though concentration contrasts between the surface and the deep ocean are much greater than for Cr. The oligotrophic nature of the South Pacific Gyre, with very low biological productivity, is driven by the strong depletion of macronutrients and essential micronutrients such as Fe (e.g. Halm et al., 2012; Ellwood et al., 2018). In turn, low biological productivity explains the minimal structure observed for other nutrient-type elements that are not completely exhausted in surface waters, such as Cr. The homogenous δ^{53}Cr values (within analytical uncertainty) observed along GP13 are consistent with the limited range of [Cr] in upper waters and the tight correlation between [Cr] and δ^{53}Cr in the global ocean.

Considering the oligotrophic environment and the already muted nutrient-type Cr distribution compared to other nutrient-type elements, biological impacts on Cr are expected to be minimal, as noted above. Nevertheless, some profiles do show subtle features that may be associated with biological control. Stations with a chlorophyll maximum in the mixed layer (Stns 3–18) show surface or near-surface [Cr] minima, while stations with a chlorophyll maximum below the mixed layer show a minor [Cr] minimum at the depth of the deep chlorophyll maximum (e.g. Stns 23 & 28) (Fig. 2). These features (~0.1 nmol kg^{-1}) are only slightly more prominent than the uncertainty (1% RSD) and are also not resolved at all stations. Therefore, these trends are interpreted with caution, but they offer support to biologically-driven distributions reported in more productive regions (Goring-Harford et al., 2018; Janssen et al., 2020).

In addition to these chlorophyll-relatable Cr minima, the two stations nearest to the Australian coast (Stns 3 & 8) show a slight [Cr] maximum (~0.15 nmol kg^{-1}) at the shallowest sampled depth(s) (Fig. 2). Due to the proximity of these stations to the Australian continent, it is possible that a local source enriches Cr in the uppermost waters. Such a contribution, associated with the continental shelf and atmospheric deposition, was observed for [Fe] along the transect (Ellwood et al., 2018; Cabanes et al., 2020). Potential atmospheric deposition of Cr can be estimated from soluble Fe and Al deposition in the region (Ellwood et al., 2018),

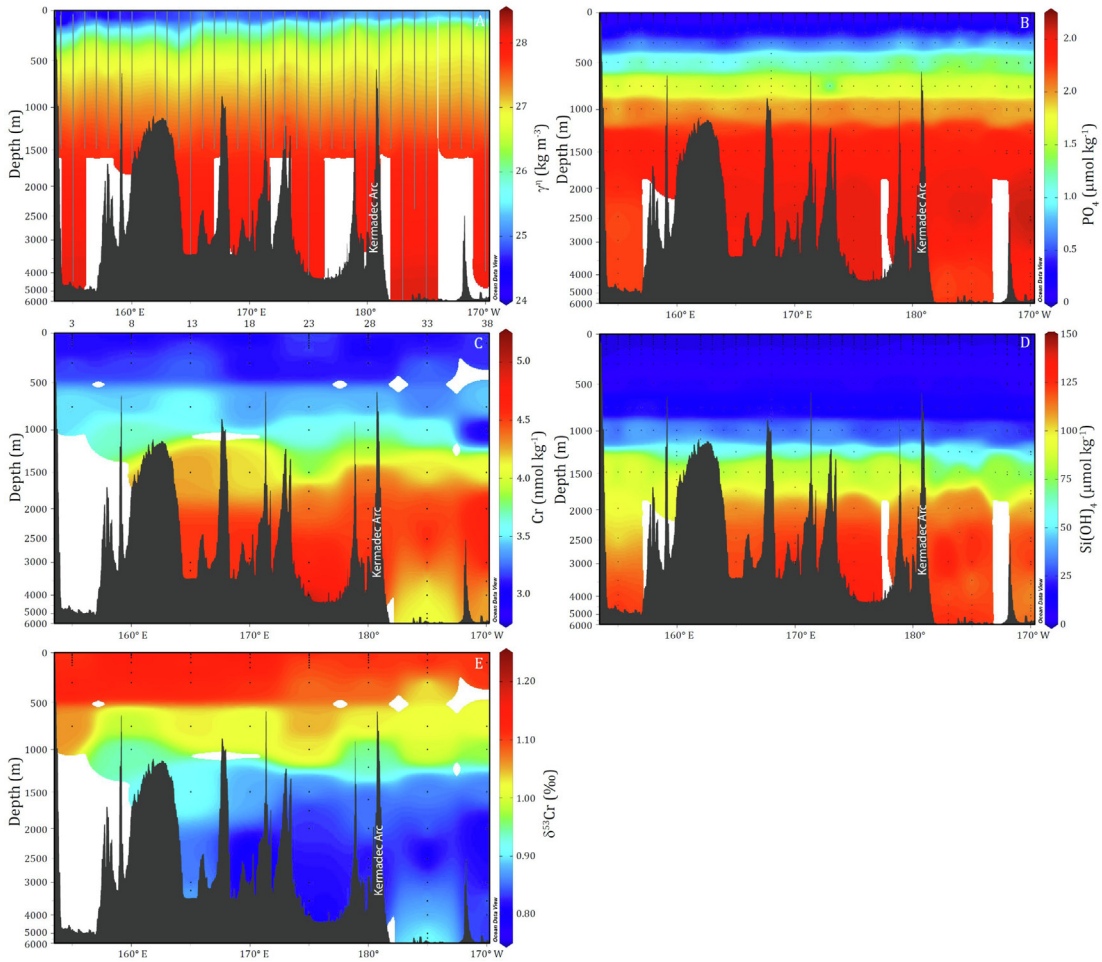

Fig. 3. GP13 section plots of hydrography, macronutrient concentrations, [Cr] and δ^{53}Cr. (A) Neutral Density (γ^n), (B) PO_4, (C) Cr, (D) $Si(OH)_4$, (E) δ^{53}Cr. Note the non-linear depth scales. Locations of CTD data are shown as grey lines in A, discrete sample depths for geochemical data as black circles.

assuming crustal Cr/Fe and Cr/Al (Rudnick & Gao, 2003) (see Appendix A.1). By necessity, this calculation makes significant approximations – i.e. that measured Fe and Al fluxes along the transect are representative of annual fluxes and that Cr solubility matches that of Fe and Al. Nevertheless, regional deposition of Fe and Al indicates that it would take decades to result in the excess Cr of ~0.15 nmol kg^{-1} seen in the uppermost depths, and therefore atmospheric deposition is an unlikely explanation. Based on the presently available data, there is no clear explanation for the apparent surface Cr maxima at stations 3 and 8.

5.2. Intermediate and Deep Waters

Increases in Cr and decreases in δ^{53}Cr below the euphotic zone match transitions in water masses from predominantly Subtropical Surface and Mode Waters to southern-sourced intermediate waters (Fig. 3). Chromium concentrations and δ^{53}Cr in AAIW along GP13 are equivalent to Southern Ocean values (along GP13: [Cr] = 3.50 ± 0.12 and δ^{53}Cr to 1.01 ± 0.07, 1 SD and 2 SD respectively, n = 12; Southern Ocean [Cr] = 3.62 ± 0.08, δ^{53}Cr = 0.96 ± 0.06, n = 16; Rickli et al., 2019; Janssen et al., 2021). Therefore, these trends in [Cr] and δ^{53}Cr can be explained by horizontal advection of AAIW, rather than vertical processes (e.g. particle export and Cr release, vertical mixing). This supports previous studies highlighting the role of circulation in shaping Cr distributions throughout the ocean (e.g. Moos & Boyle, 2019; Rickli et al., 2019; Janssen et al., 2021).

GP13 deep waters ([Cr] = 4.35 ± 0.27 at stations 13–23, below 1500 m and >100 m off the seafloor), corresponding to depths of CDW and PDW, have accumulated Cr during advection from the Southern Ocean (Southern Ocean CDW [Cr] = 3.88 ± 0.11, n = 32; Rickli et al., 2019; Janssen et al., 2021); however the two are isotopically indistinguishable (GP13: δ^{53}Cr = 0.86 ± 0.07; Southern Ocean: δ^{53}Cr = 0.89 ± 0.08, n = 32; Rickli et al., 2019; Janssen et al., 2021). The absence of a clear shift in δ^{53}Cr can be explained, at least partly, by the small relative increase in [Cr] (~0.45 nmol kg^{-1}, or about 10% of [Cr]). The prevalence of bathymetric features reaching into the upper 1000 m and, at times, into the upper 100 s of m in the southwest Pacific (Figs. 1 and 3) results in complex circulation patterns for CDW reaching the GP13 transect. Circumpolar Deep Water reaches stations 13–23 from distinct branches of southward flow following northward advection east of New Zealand. Consequently, the accumulation of Cr is unlikely due to one specific local point source, and instead probably results from one (or more) general mechanism(s) acting to control Cr distributions on regional to global scales.

One such global control on deep water [Cr] is a benthic Cr release (e.g. Jeandel & Minster, 1987; Janssen et al., 2021). The aforementioned bathymetric features may increase the potential for benthic sources to impact intermediate and deep waters during transit, which, along with mixing with PDW, increases [Cr] in GP13 deep water relative to CDW. Another potential global control is the release of Cr from sinking particles (Janssen et al., 2021). The low productivity in the region suggests that local Cr release from

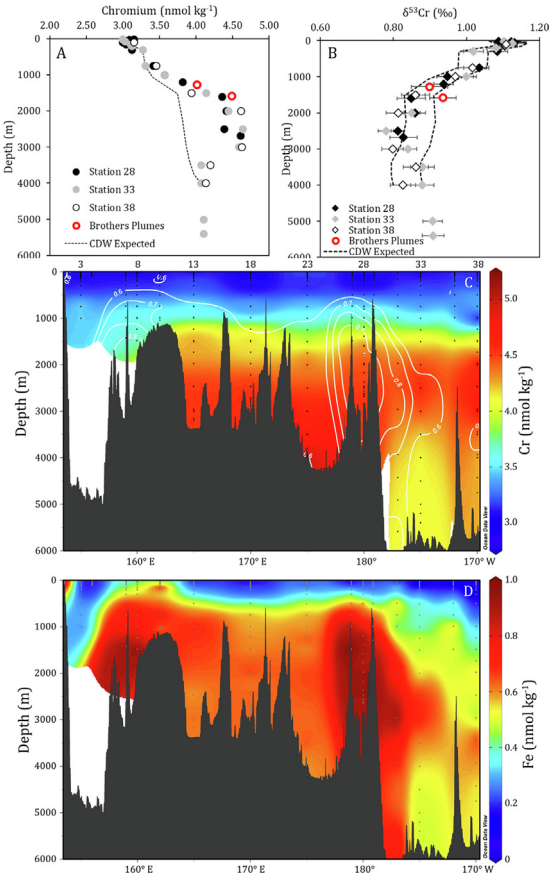

Fig. 4. Cr enrichments near the Kermadec Arc. Chromium concentrations (A) and δ^{53}Cr (B) are shown for stations 28–38 as well as Brothers Volcano plume samples. The dashed lines in (A) and (B) show average density-adjusted subantarctic South Pacific Cr distributions from >1000 m (Janssen et al., 2021), away from hydrothermal input. GP13 Station 33 data were used for ≤ 1000 m. δ^{53}Cr is shown as a 2SD range. Section plots of [Cr] (C) and [Fe] (D) are shown for the GP13 transect. The contours on panel C show [Fe] to help identify the Kermadec Arc hydrothermal plume. Iron data are from Ellwood et al. (2018; as included in the GEOTRACES IDP 2021, GEOTRACES Intermediate Data Product Group, 2021).

sinking biogenic particles is unlikely to explain Cr accumulation in deep waters along the GP13 transect. However, water column release from biogenic particles may explain some of the observed enrichment through mixing with older deep waters with Cr accumulated over longer time scales, as indicated by the elevated ^{14}C age of GP13 deep waters relative to the Southern Ocean (Gebbie and Huybers, 2012; see also Sections 2.2 and 5.3). Chromium accumulation in deep waters better matches that of Si than NO_3 and PO_4 along GP13 (Fig. 5), as identified previously in the global ocean (e.g. Jeandel & Minster, 1987; Janssen et al., 2021). This supports the prominent role of benthic processes, known to modulate [Si $(OH)_4$] (Tréguer & de la Rocha, 2013), in shaping [Cr] (Janssen et al., 2021). Multiple hydrothermal systems are known in the region near the flow path of CDW. For example, the Kermadec Arc (e.g. de Ronde et al., 2001) and the North Fiji Basin (e.g. Bendel et al., 1993) may be Cr sources (Fig. 1). In addition to potential direct input, these systems may serve as indirect Cr sources through benthic fluxes from hydrothermal sediments (Bauer et al., 2019), which may be enhanced by the complex regional bathymetry as discussed above. Broad [Fe] enrichment at these same stations supports the notion of hydrothermal (either local or distal) and/or benthic input sources (Ellwood et al., 2018; Cabanes et al., 2020).

With the exception of stations 33 and 38, the highest [Cr] and lowest δ^{53}Cr are found in the deepest sample(s) (Fig. 2), a trend observed elsewhere in the global ocean (e.g. Murray et al., 1983; Jeandel & Minster, 1987; Janssen et al., 2021). The accumulation of isotopically light Cr in these bottom-most samples also implies an isotopically light benthic flux of Cr. Such a flux may be spatially heterogeneous, and therefore have a greater local effect at some sites, but would also act to enrich deep waters along circulation pathways. A light benthic source is consistent with estimates of pore water Cr isotope compositions (Janssen et al., 2021), and is also expected due to the isotopic composition of lithogenic material (Schoenberg et al., 2008) and Cr release from biogenic particles (Janssen et al. 2021). Therefore the deepest samples support that benthic Cr fluxes may be significant (Murray et al., 1983; Jeandel & Minster, 1987; Janssen et al., 2021; Pöppelmeier et al., 2021). The stations that deviate from these bottom [Cr] maxima and δ^{53}Cr minima are discussed below in Section 5.3.

5.3. Hydrothermal influence along the GP13 transect

The GP13 section crosses the hydrothermally active Kermadec Arc system near 180° (Fig. 1; de Ronde et al., 2001; Kleint et al., 2019, 2022; Neuholz et al., 2020). A strong hydrothermally-sourced local elevation in [Fe] is seen where the GP13 transect crosses the Kermadec Arc system (station 28). The [Fe] enrichment relative to seawater background near the ridge (up to ~100%) extends from < 1000 m to > 3000 m, with a maximum around 2000–3000 m depth, as well as in a plume spreading eastward at about 3000 m depth, reaching at least to station 33 (175° W) (Ellwood et al., 2018; Fig. 4C). Multiple specifically characterized vent sites along the Kermadec Arc (e.g. Brothers, Healy, Harve, Rumble II W) and more diffuse particle-rich plumes near the base of vent sites (2000–3000 m) (de Ronde et al., 2001; Baker et al., 2003: de Ronde et al., 2007; Kleint et al, 2019), as well as long-distance transport from deep venting sites along the East Pacific Rise (Fitzsimmons et al., 2014; Resing et al., 2015) may act as potential sources of [Fe] and other metals. Elevated dissolved [Cr] is also seen over this depth range (~1500–3500 m) at stations 28–38 (Figs. 4 and 6), pointing to potential hydrothermal sources of Cr. Due to the smaller relative [Cr] enrichments over similar water masses in the Southern Ocean (up to ~17%) compared to [Fe] (>50%), the extent of the [Cr] enrichment is more difficult to discern and the source of the [Cr] enrichment is less clear. However, these data showing the highest [Cr] in hydrothermally influenced waters (Figs. 4 and 6) indicate that local vents are unlikely to be a net sink of Cr, as proposed for hydrothermal vents in general (Jeandel & Minster, 1984, 1987; Trocine & Trefry, 1988; Rudnicki & Elderfield, 1993; Feely et al., 1994). The extent to which this apparent plume of [Cr]-enriched water reflects a hydrothermal Cr source, or other sources of Cr to deep waters, is investigated by analysis of high-temperature vent and near-vent plume samples and by comparison with Southern Ocean and Pacific Ocean deep waters.

5.3.1. Vent and plume samples from the Brothers Volcano (Kermadec Arc)

Three high-temperature vent sites (representing an estimated 85–92% pure vent endmembers, based on [Mg]), as well as near-vent neutrally buoyant plume samples from the Brothers Volcano site, along the Kermadec Arc (Fig. 1), were analyzed for [Cr] and δ^{53}Cr. High-temperature vent samples show distinct Cr compositions, with [Cr] well above seawater concentrations (ranging from 7.5 to 22.3 nmol kg^{-1}), similar to previous data from the East Pacific Rise (Jeandel & Minster, 1984), and with isotopically light Cr (δ^{53}Cr = −0.07 ± 0.10‰ to +0.04 ± 0.04‰, 2SEM) (Table 2). This is similar to or slightly heavier than the average crustal (δ^{53}Cr = −0.12 ± 0.10, 2SD; Schoenberg et al., 2008) and upper mantle (δ^{53}Cr = −0.14 ± 0.12, 2SD; Xia et al., 2017) composition. δ^{53}Cr is invariable

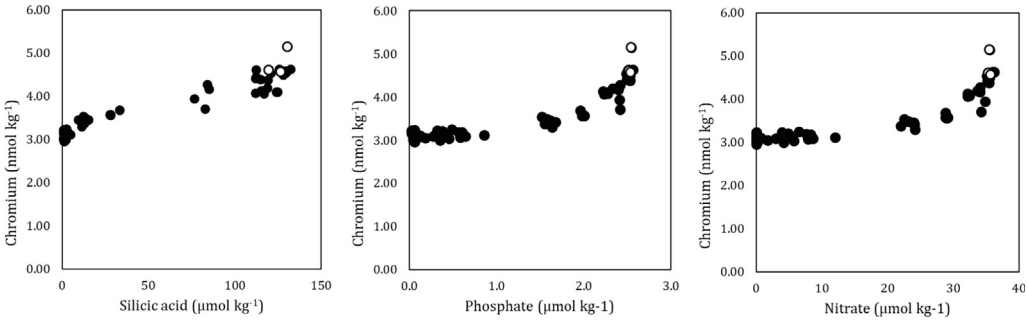

Fig. 5. Crossplots of Cr and macronutrients. Chromium is plotted against silicic acid (A), phosphate (B) and nitrate (C) to identify shared controls for Cr and macronutrients (e.g. benthic fluxes, release from biogenic particles, circulation). Chromium more closely follows Si, suggesting benthic fluxes may be important in shaping distributions. Open symbols indicate the deepest samples at stations 18–28, highlighting potential trends related to benthic sources.

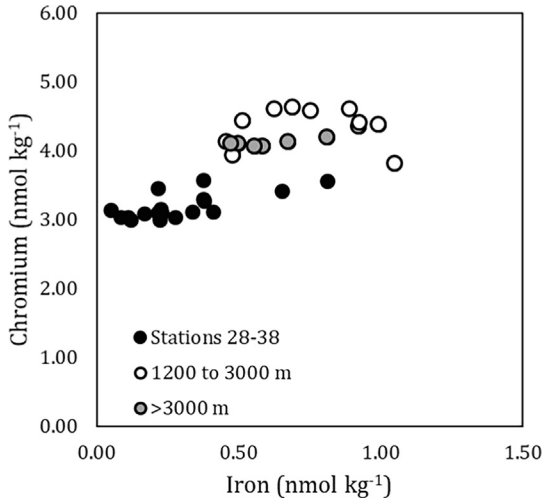

Fig. 6. Cross plot of [Cr] and [Fe] at stations 28–38. White symbols show data from 1200 to 3000 m depth, and grey symbols show data below 3000 m depth. All other data are shown in black. Iron data are from Ellwood et al. (2018). The highest [Cr] do not correspond with the highest [Fe], suggesting the two may not share the same set of dominant driving forces.

between sites, considering analytical uncertainty, and no clear trends are observed between [Cr] and temperature, salinity, pH, Eh, or vent endmember fractions. Near-vent neutrally buoyant plume samples (Table 2, Fig. 4), which are diluted > 10^2 compared to pure hydrothermal vent endmembers (Neuholz et al., 2020), yield [Cr] = 4.01 and 4.49 nmol kg^{-1} and δ^{53}Cr = 0.90 ± 0.05‰ and 0.94 ± 0.04‰ (1278 and 1584 m, respectively). These [Cr] and δ^{53}Cr values are similar to equivalent depths along GP13.

These data indicate that high-temperature vents along the Kermadec Arc may be a local source of isotopically light Cr, with potential for variability in the specific impact of different venting sites, as observed previously for other elements (Kleint et al., 2019, 2022). However, given that pure vent [Cr] is estimated to be on the order of 10–30 nmol kg^{-1} (Table 3), it is unlikely that hydrothermal fluids from the Kermadec Arc, when diluted 10^3-fold or more (i.e. [Cr] contribution of $\leq$ 0.01 nmol kg^{-1}), have a detectable impact on [Cr], and these vents are not a major Cr source overall. Despite the light isotopic composition of vent-derived Cr, near-vent water column samples are isotopically heavy, similar to intermediate and deep water δ^{53}Cr along GP13, in the Southern Ocean (e.g. Rickli et al., 2019; Janssen et al., 2021) and in the subtropical North Pacific (Moos & Boyle, 2019). The mismatch in δ^{53}Cr between nearly pure vent endmembers (δ^{53}Cr = + 0.04 ± 0.04‰ to −0.07 ± 0.10‰, 2SEM) and ambient seawater δ^{53}Cr supports interpretations that the net hydrothermal impact is likely small relative to total dissolved [Cr].

Estimates for total Fe and Mn fluxes from the Kermadec Arc, based on the Brothers Volcano site, range from 1 × 10^7 to 5 × 10^{10} mols yr^{-1} (for Fe) and from 4 × 10^7 to 6 × 10^9 mols yr^{-1} (for Mn), comparable to or higher than metal fluxes from other vent environments (Neuholz et al., 2020). First-order estimates of Cr fluxes in the Kermadec Arc based on Cr/Fe and Cr/Mn in Brothers Volcano vent fluids are even less certain due to variations in these ratios of ~1 order of magnitude (Table 3). However, as Cr/Fe and Cr/Mn are ~1 × 10^{-6} (plus or minus one order of magnitude), this suggests approximate Cr fluxes of ~10 to 10^4 mols Cr yr^{-1}. Despite the large uncertainties in both the original Fe and Mn fluxes, and in converting this to Cr fluxes, these estimates indicate that hydrothermal Cr contributions are unlikely to be of global importance relative to other components of the Cr cycle (major sources ~10^8 mols Cr yr^{-1}, e.g. Pöppelmeier et al., 2021).

5.3.2. Comparison of GP13 deep water with available Southern Ocean and Pacific Deep Water data

These high temperature vent data suggest negligible hydrothermal Cr contributions at stations 28–38 along GP13, despite Fe suggesting a local point source (Fig. 4), and instead a dominant control by water mass mixing. This can be assessed by estimating expected Cr systematics based on the relevant regional water masses (CDW, PDW) away from GP 13. While waters above and below the hydrothermally-impacted depth range along GP13 converge with the hydrographic properties of Southern Ocean and subantarctic waters, the hydrographic properties of hydrothermally-influenced depths lie between CDW and PDW (Fig. 7), indicating an influence of PDW. This can also be seen in ^{14}C water mass ages in the region showing older waters along the GP13 transect compared to CDW (Gebbie and Huybers, 2012). However, the nearest PDW-influenced seawater data that could constrain expected PDW Cr systematics at GP13 are from the subtropical North Pacific (Moos & Boyle, 2019), nearly 9000 km away from GP13. Conservative advection cannot be assumed over this spatial scale due to the non-conservative nature of Cr, with external sources (e.g. benthic fluxes) and internal cycling (e.g. release from particles) acting to increase [Cr] as water masses age (e.g. Jeandel & Minster, 1987; Janssen et al., 2021). However, to a first order, GP13 deep water [Cr] at stations 28–38 is generally comparable to or slightly less than PDW [Cr] in the North Pacific (Fig. 7).

Due to the lack of relevant PDW Cr data in the region, we calculate total Cr accumulated along GP13 compared to CDW to the south of the transect (UCDW: [Cr] = 3.82 ± 0.07 nmol kg^{-1} (1SD) and δ^{53}Cr = 0.90 ± 0.08‰ (2SD), n = 20; LCDW: [Cr] = 3.97 ± 0.1 n mol kg^{-1} (1SD) and δ^{53}Cr = 0.86 ± 0.07‰ (2SD), n = 12; data from

Table 3
Estimated pure hydrothermal endmembers.

Sample	[Cr] nmol kg^{-1}
SO253_067_ROV_11F	27
SO253_064_ROV_5F	8
SO253_081_ROV_3F	9

Pure hydrothermal endmembers are estimated by mass balance from measured hydrothermal vent samples and estimated endmember% (Table 2) and assuming conservative mixing with a background seawater of [Cr] = 3.90 nmol kg^{-1}.
$[Cr]_{endmember} = \left([Cr]_{measured} - 3.90\,nmol\,kg^{-1} \times \left(1 - \frac{\%_{endmember}}{100}\right)\right) \div \frac{\%_{endmember}}{100}$.
This calculation is necessarily approximate because the assumption of conservative mixing may not be true and because the background seawater signal is not precisely known (see Section 5.3). In order to avoid a false sense of precision, an uncertainty is not presented here. For the same reasoning, an endmember $\delta^{53}Cr$ is not estimated, though given this relative purity of the high-temperature fluids, the endmember $\delta^{53}Cr$ is expected to be similar.

Rickli et al., 2019; Janssen et al., 2021). This integrates multiple potential Cr sources related to water mass transport and aging (release from sinking particles, benthic fluxes; Janssen et al., 2021), as well as potential hydrothermal sources, although they are likely small (Section 5.3.1). Taking our samples with the greatest Cr accumulation at stations 28–38 (1600–3000 m at stations 28–38, n = 9), the total accumulated Cr ($[Cr]_{accumulated}$) and $\delta^{53}Cr$ ($\delta^{53}Cr_{accumulated}$) are calculated following standard mass balance equations (Eqs. (1) and (2), Table 1).

$$[Cr]_{GP13} = ([Cr]_{CDW} + [Cr]_{accumulated}) \quad (1)$$

$$\delta^{53}Cr_{GP13} \times [Cr]_{GP13} = (\delta^{53}Cr_{CDW} \times [Cr]_{CDW} + \delta^{53}Cr_{accumulated} \times [Cr]_{accumulated}) \quad (2)$$

The average $[Cr]_{accumulated}$ is 0.71 ± 0.11 nmol kg^{-1} (1SD), with a maximum of approximately 0.8 nmol kg^{-1} at 2000–2500 m depth, with a $\delta^{53}Cr_{accumulated}$ = +0.46 ± 0.30‰ (2SD, n = 9, Table 1).

Even a relatively minor dilution of vent fluids (10^1 nmol Cr kg^{-1}) by 10^2 would result in a vent contribution of Cr that is small relative to the total accumulated ~0.7 nmol kg^{-1}. As such a dilution factor is only likely very close to the vents (e.g. Neuholz et al., 2020), and samples along GP13 are likely diluted orders of magnitude more than this, the resulting vent-derived Cr contributions ($\leq 10^{-2}$ nmol kg^{-1} Cr) are insignificant relative to other sources. The curved [Cr]–[Fe] trend in these samples, indicating the primary control on these metals is not shared (Fig. 6), further supports the importance of other processes in shaping Cr. Considering more distal sources such as the East Pacific Rise, the general uniformity of the observed elevated [Cr], while [Fe] shows the decrease of a point or regional source east of 180° (Figs. 4, 6 and 7), suggests distal hydrothermal sources are an unlikely explanation of Cr trends. Finally, $\delta^{53}Cr_{accumulated}$ (+0.46 ± 0.30‰) agrees with benthic fluxes and release from sinking particles (~0.3‰ Janssen et al., 2021), but differs from high temperature fluid $\delta^{53}Cr$ (+0.08 to −0.17‰). Therefore, supporting high temperature and near-vent data, hydrothermal vent sources are unlikely to drive our observations along GP13, which instead reflect processes acting as water masses age such as benthic fluxes and release from particles, as well as water mass transport and mixing.

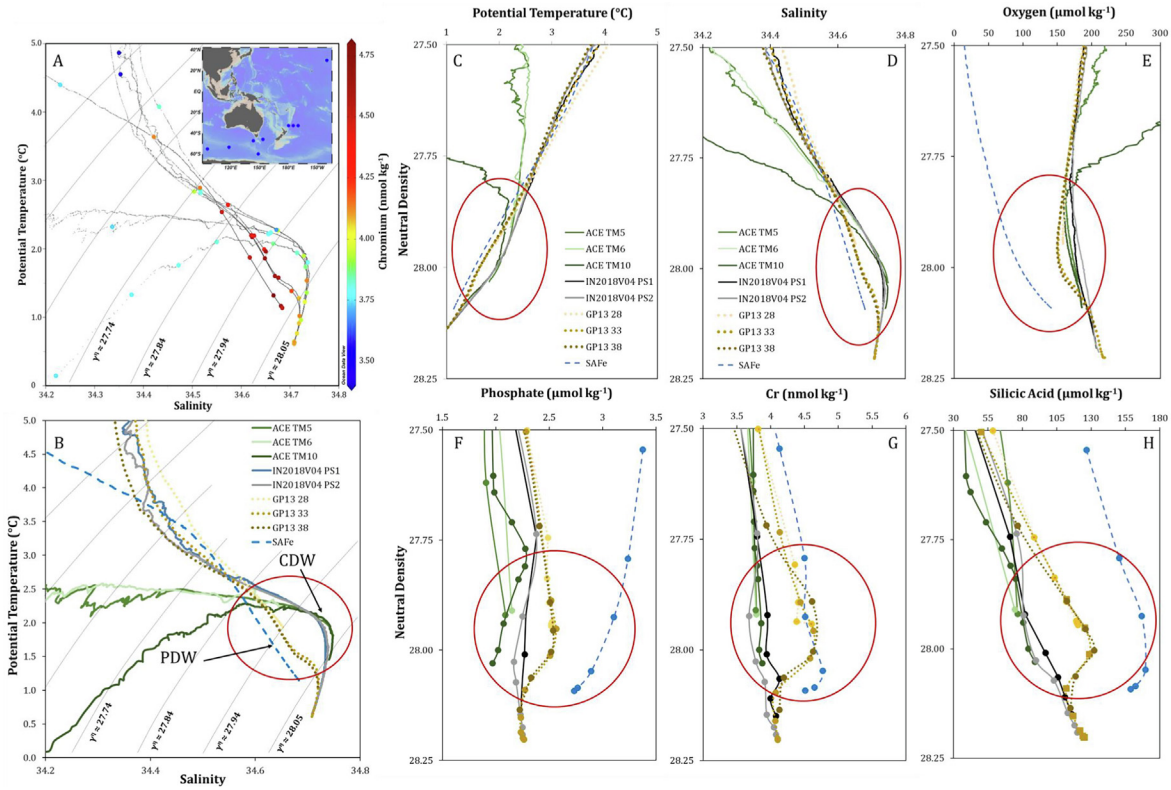

Fig. 7. Hydrographic and chemical properties of GP13 deep waters along with Circumpolar and Pacific Deep Water. Main hydrographic properties (temperature, salinity and neutral density, Panels A-D) identify deviations of GP13 from the hydrographic properties of Southern Ocean and subantarctic deep waters (encircled in red). Also shown are oxygen (E), [PO_4] (F), [Cr] (G) and [Si] (H) profiles against neutral density. Discreet sample depths are shown as circles for macronutrient and Cr data (A, C–G). Contour lines in (A) and (B) denote potential density isopycnals, with labels reflecting approximate equivalent neutral density (γ^n). Note that γ^n depends on geographic location and therefore this presentation is, by necessity, imprecise. Isopycnal contours are provided only as an approximate guide and not meant to be quantitative. Southern Ocean (ACE Legs 1 & 2, Rickli et al., 2019; Janssen et al., 2021, green solid lines) and subantarctic (IN2018V04, Janssen et al., 2021, grey and black solid lines) data are compared to the GP13 transect (yellow dotted lines, this study) and North Pacific data (Moos & Boyle, 2019, blue dashed lines) (stations shown in inset map in Panel A).

5.4. Implications of hydrothermal input on the Cr cycle and paleoceanographic interpretations

While the overall magnitude of the potential Cr source along the Kermadec Arc and the GP13 transect is small, restricting its impact to only vent-proximal sites, enrichments of [Cr] are observed in high-temperature vent fluids, along with the absence of [Cr] depletion in hydrothermally-impacted waters. Therefore, hydrothermal systems are likely a net source rather than a net sink, as some previous studies have suggested (Jeandel & Minster, 1984; Rudnicki & Elderfield, 1993), at least at the Kermadec Arc, though this is small relative to other sources (see Section 5.3.2). The extent to which our results from the Kermadec Arc are applicable to other hydrothermal systems, including whether global hydrothermal fluxes in composite are a net Cr source or sink, may depend on differences in vent chemistry across diverse systems, and should be investigated further. For example, the specific vent chemistry will regulate the flux of known Cr reductants (e.g. Fe(II) and sulfides, Pettine et al., 1998; Kim et al., 2001) into the water column, which may influence how much ambient Cr may be reduced and scavenged out. It is possible that the low Fe/Mn and high Fe/H_2S (i.e. lower availability of Cr reductants such as Fe(II) and sulfides, see Section 2.3, Kleint et al., 2022) observed at multiple vent sites on the Kermadec Arc (Kleint et al., 2019, 2022) result in improved stability of Cr in the hydrothermal plume and minimize the reduction and removal of ambient seawater Cr after mixing with plume waters. However, the high variability of high-temperature vent fluid chemistry within the southern Kermadec Arc (Kleint et al., 2019) complicates a mechanistic understanding of which specific conditions may allow for the accumulation of dissolved Cr in the neutrally buoyant hydrothermal plume.

Our observations also constrain the net impact of hydrothermal fluxes at the Kermadec Arc in terms of Cr isotopes. The elevation in seawater [Cr], both near Brothers Volcano vents and along GP13 does not produce a clear departure from the δ^{53}Cr–ln(Cr) trend of global data (Fig. 8). This reflects that the enrichment over Southern Ocean CDW is not large (<20%), and is overwhelmingly attributable to non-hydrothermal sources. When considering the high-temperature vent samples (Fig. 8 yellow circles), greater departures are seen from global δ^{53}Cr–[Cr] systematics, though the projection of the trend from normal oceanic samples falls between the three hydrothermal samples. Conservative mixing is not a Rayleigh-type process; therefore mixing of seawater with these hydrothermal endmember fluids would fall below the linear Rayleigh trend (dashed line in Fig. 8). Nevertheless, the general similarity in hydrothermal and global seawater Cr systematics – low δ^{53}Cr associated with high [Cr] suggests the net effect of hydrothermal Cr input may still not be far from the trend illustrated by the global seawater array, even for ocean waters with a strong hydrothermal influence.

There is increasing interest in δ^{53}Cr records as indicative of hydrothermalism in the paleocean (e.g. Holmden et al., 2016; Bauer et al., 2021; Yobo et al., 2022). Our hydrothermal data provide the first isotopic constraints on hydrothermally sourced Cr (δ^{53}Cr = −0.17 to +0.08‰), yielding compositions comparable to the upper continental crust and the upper mantle (−0.26 to −0.02‰; Xia et al., 2017). These observations support previous assumptions that the two pools are equivalent and that increased input of hydrothermally-sourced Cr to seawater should therefore drive ocean δ^{53}Cr to lighter values, where this low δ^{53}Cr water signal may then be captured in authigenic sedimentary reservoirs (e.g. Holmden et al., 2016; Bauer et al., 2021; Yobo et al., 2022). However, given high-temperature vent endmember [Cr] of around 10–30 nmol kg^{-1}, our data indicate that hydrothermal vents are not likely to be a major source of Cr to the ocean. Therefore orders of magnitude-level changes in hydrothermal cycling would still not overwhelm the roles of other oceanic processes shaping δ^{53}Cr distributions, except perhaps in immediate proximity to vent systems. Recent δ^{53}Cr data from redox-stratified basins, showing that isotopically light Cr accumulates in anoxic zones (Janssen et al., 2022), provide an alternate mechanism for lowered seawater δ^{53}Cr during expanded deep water anoxia – the expansion and intensification ocean anoxia should enhance the accumulation of dissolved isotopically light Cr, which may then be reflected in sediment records. In summary, Cr distributions may be more sensitive to other drivers, and δ^{53}Cr records from ocean anoxic events with increased hydrothermal activity may more likely reflect internal processes such as widespread anoxia, instead of or in addition to increased external hydrothermal sources.

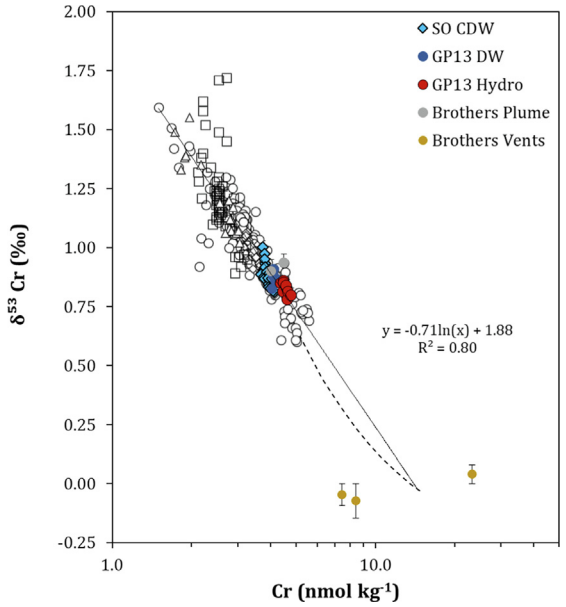

Fig. 8. δ^{53}Cr-lnCr array. Global ocean Cr data are shown for the Pacific (circles), Southern (diamonds), Atlantic (squares) and Arctic (triangles) Oceans, with Brothers Volcano vent samples as yellow circles and plume samples in grey circles. The Rayleigh fractionation trendline is a linear fit to all data except Brothers vent samples, with slope and r^2. Hydrothermally-influenced CDW (red) along GP13 (stations 28–38, 1600–3000 m) and in the Brothers Volcano neutrally-buoyant plume are compared to CDW in the Southern Ocean (light blue diamonds) and deep waters along GP13 (dark blue circles). The dashed line indicates conservative mixing between the extended linear projection near hydrothermal endmembers and deep waters along GP13. Data sources: Scheiderich et al., 2015; Goring-Harford et al., 2018; Moos & Boyle, 2019; Rickli et al., 2019; Janssen et al., 2020; Moos et al., 2020; Nasemann et al., 2020; Huang et al., 2021; Janssen et al., 2021. Low salinity data, data restricted to coastal regions, and data highlighted as suspect by subsequent studies are not shown.

6. Conclusions

We report new dissolved [Cr] and δ^{53}Cr data from the GEOTRACES GP13 section in the southwest subtropical Pacific Ocean, extending eastward from the Australian seaboard to the open, subtropical Pacific Gyre. Depth profiles reflect nutrient-type elemental distributions, with lower [Cr] in surface waters and elevated [Cr] at depth. δ^{53}Cr largely mirrors [Cr], and shows surface δ^{53}Cr maxima and minima in deep waters. Although surface minima in [Cr] are a consistent feature throughout the transect, these minima reflecting seasonal biological uptake above the winter mixed layer are subtle in this low productivity, oligotrophic region. Similar trends are observed for macronutrients and other nutrient-type trace metals (Ellwood et al., 2018; George et al., 2019; Cabanes et al., 2020). Elevated [Cr] and low δ^{53}Cr at depth largely reflect transitions between water masses, and are explained by the advection of

nutrient- and Cr-rich intermediate and deep waters from the Southern Ocean and the Pacific. Local maxima near the sediments indicate benthic sources of Cr throughout the transect, supporting previous interpretations of benthic sources in the North Pacific and the Atlantic (Murray et al., 1983; Jeandel & Minster, 1987) as well as recent pore water and modelling data indicating that benthic fluxes may represent a large local and global source of Cr (Janssen et al., 2021; Pöppelmeier et al., 2021).

Based on box models and near-vent particles and sediments, previous studies have indicated that hydrothermal vents may be a net sink of Cr rather than a net source (Jeandel & Minster, 1984; Jeandel & Minster, 1987; Trocine & Trefry, 1988; Rudnicki & Elderfield, 1993; Feely et al., 1994; Bauer et al., 2019). New high-temperature vent samples and neutrally buoyant plume samples from the Brothers Volcano (Kermadec Arc) indicate elevated [Cr], suggesting this vent system is a source rather than a sink of Cr. Hydrothermal vent fluid Cr (−0.17 to +0.08‰) is isotopically similar to or slightly heavier than continental crust and the upper mantle (−0.26 to −0.02‰, Schoenberg et al., 2008; Xia et al., 2017). However, [Cr] in hydrothermal endmembers (~10–30 nmol kg^{-1}) indicates that hydrothermally-sourced Cr is unlikely to dominate Cr accumulation in deep waters after dilution with background seawater, except immediately near active vent sites. Along the GP13 section, elevated dissolved Cr is seen between 1600 and 3000 m depth east of the Kermadec Arc. Based on regional hydrography, these depths consist of a mixture of Circumpolar and Pacific Deep Waters. The average [Cr] enrichment in these waters is 0.71 ± 0.11 nmol kg^{-1} (1SD, n = 9), with an average accumulated δ^{53}Cr of +0.46 ± 0.30‰ (2SD, n = 9), which likely reflects other processes known to act in the ocean interior (e.g. release from sinking particles, benthic fluxes), and not hydrothermal sources. Overall, our observations indicate hydrothermal vents are unlikely to be a major factor controlling oceanic Cr distributions at wider scale, even with increases of multiple orders of magnitude in hydrothermal fluxes, and that large changes in other external Cr sources and/or factors controlling the oceanic Cr cycling (e.g. widespread anoxia) should be considered when interpreting δ^{53}Cr records during periods of enhanced hydrothermal input throughout Earth's history.

Data availability

All Cr data are included in a table in the Appendix (Table A.1). CTD, macronutrient and other trace metal data are available in the GEOTRACES intermediate data product (GEOTRACES Intermediate Data Product Group, 2021)).

Data availability

All Cr data are included in the main text and in the supplement.

Declaration of Competing Interest

The authors declare that they have no known competing financial interests or personal relationships that could have appeared to influence the work reported in this paper.

Acknowledgements

We thank the captains, crews, and scientific members of the RV Southern Surveyor and the Marine National Facility for making voyage SS2011_V02 a success. We thank Martin Wille for Neptune support and sharing discussions and analytical expertise, and for providing a subsample of his Merck Cr(III) standard, originally from Ronny Schoenberg. We acknowledge funding from the Swiss National Science Foundation (SNSF grant PP00P2_172915) and by a European Research Council (ERC) Consolidator Grant (SCrIPT grant agreement 819139) to SLJ. We also acknowledge the Australian Research Council for funding under the Future Fellowships scheme to ARB (FT130100037), and the Antarctic Climate and Ecosystems Cooperative Research Centre. Hydrothermal fluid samples from Brothers Volcano, Kermadec Arc, were collected during research cruise SO253 with R/V Sonne; funding of this cruise by the BMBF (German Federal Ministry of Education and Research, project 03G0253) is greatly acknowledged. We thank associate editor Rachael James, Kohen Bauer, and an anonymous reviewer for constructive comments which have improved our manuscript. Chromium data were obtained on a Neptune Plus MC-ICP-MS acquired with funds from the NCCR PlanetS supported by SNSF grant 51NF40-141881. Maps and some figures were made using Ocean Data View (available at http://odv.awi.de).

Author contributions

DJ, DG, SJ designed the study, and CS, ARB and MJ designed GP13 field sampling and provided samples. ARB led the GP13 leg 1 voyage (SS2011_V02) of RV Southern Surveyor. AK and CK contributed Brothers Volcano samples. DJ processed and analyzed Brothers Volcano samples. DJ and DG processed GP13 samples and DJ analyzed the samples. DJ, DG and SJ led interpretations of the data. All authors contributed to interpretations and to the manuscript.

Appendix A. Supplementary material

Supplementary material to this article can be found online at https://doi.org/10.1016/j.gca.2022.12.010.

References

Achterberg, E.P., van den Berg, C.M.G., 1997. Chemical speciation of chromium and nickel in the western Mediterranean. Deep-Sea Res. II 44, 693–720.
Albut, G., Babechuk, M.G., Kleinhanns, I.C., Benger, M., Beukes, N.J., Steinhilber, B., Smith, A.J.B., Kruger, S.J., Schoenberg, R., 2018. Modern rather than Mesoarchaean oxidative weathering responsible for the heavy stable Cr isotopic signatures of the 2.95 Ga old Ijzermijn iron formation (South Africa). Geochim. Cosmochim. Acta 228, 157–189.
Baker, E.T., Feely, R.A., de Ronde, C.E.J., Massoth, G.J., Wright, I.C., 2003. Submarine hydrothermal venting on the southern Kermadec volcanic arc front (offshore New Zealand): location and extent of particle plume signatures. Geol. Soc. London Spec. Pub. 219, 141–161.
Ball, J.W., Bassett, R.L., 2000. Ion exchange separation of chromium from natural water matrix for stable isotope mass spectrometric analysis. Chem. Geol. 168, 123–134.
Bauer, K., Cole, D.B., Asael, D., Francois, R., Calvert, S.E., Poulton, S.W., Planavsky, N.J., Crowe, S.A., 2019. Chromium isotopes in marine hydrothermal sediments. Chem. Geol. 529, 119286.
Bauer, K.W., Gueguen, B., Cole, D.B., Francois, R., Kallmeyer, J., Planavsky, B.N., Crowe, S.A., 2018. Chromium isotope fractionation in ferruginous sediments. Geochim. Cosmochim. Acta 223, 198–215.
Bauer, K.W., Bottini, C., Frei, R., Asael, D., Planavsky, N.J., Francois, R., McKenzie, N.R., Erba, E., Crowe, S.A., 2021. Pulsed volcanism and rapid oceanic deoxygenation during Oceanic Anoxic Event 1a. Geology 49 (12), 1452–1456.
Bendel, V., Fouquet, Y., Auzende, J.M., Lagabrielle, Y., Grimaud, D., Urabe, T., 1993. The White Lady hydrothermal field, North Fiji back-arc basin, southwest Pacific. Econ. Geol. 88, 2237–2249.
Bostock, H.C., Sutton, P.J., Williams, M.J.M., Opdyke, B.N., 2013. Reviewing the circulation and mixing of Antarctic Intermediate Water in the South Pacific using evidence from geochemical tracers and Argo float trajectories. Deep Sea Res. I. 73, 84–98.
Cabanes, D.J.E., Norman, L., Bowie, A.R., Strmecki, S., Hassler, C.S., 2020. Electrochemical evaluation of iron-binding ligands along the Australian GEOTRACES southwestern Pacific section (GP13). Mar. Chem. 219, 103736.
Caffin, M., Moutin, T., Foster, R.A., Bouruet-Aubertot, P., Doglioli, A.M., Berthelot, H., Guieu, C., Grosso, O., Helias-Nunige, S., Leblond, N., Giminez, A., Petrenki, A.A., de Verneil, A., Bonnet, S., 2018. N2 fixation as a dominant new N source in the western tropical South Pacific Ocean (OUTPACE cruise). Biogeosciences 15, 2565–2585.

Campbell, J.A., Yeats, P.A., 1981. Dissolved chromium in the northwest Atlantic Ocean. Earth Planet. Sci. Lett. 53, 427–433.
Chiswell, S.M., Bostock, H.C., Sutton, P.J.H., Williams, M.J.M., 2015. Physical oceanography of the deep seas around New Zealand: a review. New Zealand J. Mar. Fresh. Res. 49 (2), 286–317.
Davidson, A.B., Semeniuk, D.M., Koh, J., Holmden, C., Jaccard, S.L., Francois, R., Crowe, S.A., 2020. A $Mg(OH)_2$ coprecipitation method for determining chromium speciation and isotopic composition in seawater. Limnol. Oceanogr. Meth. 18, 8–19.
de Ronde, C.E.J., Baker, E.T., Massoth, G.J., Lupton, J.E., Wright, I.C., Feely, R.A., Greene, R.R., 2001. Intra-oceanic subduction-related hydrothermal venting, Kermadec volcanic arc, New Zealand. Earth Planet. Sci. Let. 193, 359–369.
de Ronde, C.E.J., Baker, E.T., Massoth, G.J., Lupton, J.E., Wright, I.C., Sparks, R.J., Bannister, S.C., Reyners, M.E., Walker, S.L., Greene, R.R., Ishibashi, J., Faure, K., Resing, J.A., Lebon, G.T., 2007. Submarine hydrothermal activity along the mid-Kermadec Arc, New Zealand: Large-scale effects on venting. Geochim. Geophys. Geosys. 8 (7).
Ellwood, M.J., Bowie, A.R., Baker, A., Gault-Ringold, M., Hassler, C., Law, C.S., Maher, W.A., Marriner, A., Nodder, S., et al., 2018. Insights into the biogeochemical cycling of iron, nitrate, and phosphate across a 5300 km South Pacific Zonal Section (153°E–150°W). Glob. Biogeochem. Cy. 32, 187–207.
Feely, R.A., Massoth, G.J., Trefry, J.H., Baker, E.T., Paulson, A.J., Lebon, G.T., 994. Composition and sedimentation of hydrothermal plume particles from North Cleft segment, Juan de Fuca Ridge. J. Geophys. Res. Solid Earth 99 (B3), 4985–5006.
Field, M.P., Sherrell, R.M., 2000. Dissolved and particulate Fe in a hydrothermal plume at 9°45′N, East Pacific Rise: Slow Fe (II) oxidation kinetics in Pacific plumes. Geochim. Cosmochim. Acta 64 (4), 619–628.
Fitzsimmons, J.N., Boyle, E.A., Jenkins, W.J., 2014. Distal transport of dissolved hydrothermal iron in the deep South Pacific Ocean. Proc. Nat. Acad. Sci. USA 111 (47), 16654–16661.
Frank, A.B., Klaebe, R.M., Löhr, S., Xu, L., Frei, R., 2020. Chromium isotope composition of organic-rich marine sediments and their mineral phases and implications for using black shales as a paleoredox archive. Geochim. Cosmichim. Act. 270, 338–359.
Frei, R., Gaucher, C., Poulton, S.W., Canfield, D.E., 2009. Fluctuations in Precambrian atmospheric oxygenation recorded by chromium isotopes. Nature 461, 250–254.
Ganachaud, A., Cravatte, S., Melet, A., Schiller, A., Holbrook, N.J., Sloyan, B.M., Widlansky, M.J., Bowen, M., Verron, J., Wiles, P., Ridgway, K., 2014. The Southwest Pacific Ocean circulation and climate experiment (SPICE). J. Geophys. Res. Oc. 119 (11), 7660–7686.
Gebbie, G., Huybers, P., 2012. The mean age of ocean waters inferred from radiocarbon observations: Sensitivity to surface sources and accounting for mixing histories. J. Phys. Ocean. 42 (2), 291–305.
George, E., Stirling, C.H., Gault-Ringold, M., Ellwood, M.J., Middag, R., 2019. Marine biogeochemical cycling of cadmium and cadmium isotopes in the extreme nutrient-depleted subtropical gyre of the South West Pacific Ocean. Earth Planet. Sci. Let. 514, 84–95.
GEOTRACES Intermediate Data Product Group, 2021. The GEOTRACES Intermediate Data Product 2021 (IDP2021). NERC EDS British Oceanographic Data Centre NOC.
Goring-Harford, H.J., Klar, J.K., Pearce, C.R., Connelly, D.P., Achterberg, E.P., James, R. H., 2018. Behaviour of chromium isotopes in the eastern sub-tropical Atlantic Oxygen Minimum Zone. Geochim. Cosmochim. Acta 236, 41–59.
Halm, H., Lam, P., Ferdelman, T.G., Lavik, G., Dittmar, T., LaRoche, J., D'Hondt, S., Kuypers, M.M.M., 2012. Heterotrophic organisms dominate nitrogen fixation in the South Pacific Gyre. ISME J. 6, 1238–1249.
Holmden, C., Jacobson, A.D., Sageman, B.B., Hurtgen, M.T., 2016. Response of the Cr isotope proxy to Cretaceous Ocean Anoxic Event 2 in a pelagic carbonate succession from the Western Interior Seaway. Geochim. Cosmochim. Acta 186, 277–295.
Horner, T.J., Little, S.H., Conway, T.M., Farmer, J.R., Hertzberg, J.E., Janssen, D.J., Lough, A.J.M., McKay, J.L., Tessin, A., Galer, S.J.G., Jaccard, S.L., Lacan, F., Paytan, A., Wuttig, K., GEOTRACES-PAGES Biological Productivity Working Group Members, 2021. Bioactive trace metals and their isotopes as paleoproductivity proxies: An assessment using GEOTRACES-era data. Glob. Biogeochem. Cy. 35 (11). e2020GB006814.
Huang, T., Moos, S.B., Boyle, E.A., 2021. Trivalent chromium isotopes in the eastern tropical North Pacific oxygen-deficient zone. Proc. Nat. Acad. Sci. USA 118 (8). e1918605118.
Hug, S.J., Laubscher, H.-U., 1997. Iron(III) catalyzed photochemical reduction of chromium(VI) by oxalate and citrate in aqueous solutions. Environ. Sci. Tech. 31, 160–170.
Janssen, D.J., Rickli, J., Wille, M., Steiner, O.S., Vogel, H., Dellwig, O., Berg, J.S., Bouffard, D., Lever, M.A., Hassler, C.S., Jaccard, S.L., 2022. Chromium cycling in redox-stratified basins challenges $\delta^{53}Cr$ paleoredox proxy applications. Geophys. Res. Let. 49 (21). e2022GL099154.
Janssen, D.J., Rickli, J., Quay, P.D., White, A.E., Nasemann, P., Jaccard, S.L., 2020. Biological control of chromium redox and stable isotope composition in the surface ocean. Glob. Biogeochem. Cy. 34.
Janssen, D.J., Rickli, J., Abbott, A.N., Ellwood, M.J., Twining, B.S., Ohnemus, D.C., Nasemann, P., Gilliard, D., Jaccard, S.L., 2021. Release from biogenic particles, benthic fluxes, and deep water circulation control Cr and $\delta^{53}Cr$ distributions in the ocean interior. Earth Planet Sci Let. 574, 117163.
Jeandel, C., Minster, J.F., 1984. Isotope dilution measurement of inorganic chromium (III) and total chromium in seawater. Mar. Chem. 14 (4), 347–364.
Jeandel, C., Minster, J.F., 1987. Chromium behavior in the ocean: global versus regional processes. Global Biogeochem. Cy. 1, 131–154.
Kieber, R.J., Helz, G.R., 1992. Indirect photoreduction of aqueous chromium(VI). Environ. Sci. Tech. 26, 307–312.
Kiefer, D.A., Chamberlin, W.S., Booth, C.R., 1989. Natural fluorescence of chlorophyll a: Relationship to photosynthesis and chlorophyll concentration in the western South Pacific gyre. Limnol. Oceanogr. 34 (5), 868–881.
Kim, C., Zhou, Q., Deng, B., Thornton, E.C., Xu, H., 2001. Chromium(VI) Reduction by Hydrogen Sulfide in Aqueous Media: Stoichiometry and Kinetics. Environ. Sci. Tech. 35 (11), 2219–2225.
Kleint, C., Bach, W., Diehl, A., Fröhberg, N., Garbe-Schönberg, D., Hartmann, J.F., de Ronde, C.E.J., Sander, S.G., Strauss, H., Strucker, V.K., Thal, J., Zitoun, R., Koschinsky, A., 2019. Geochemical characterization of highly diverse hydrothermal fluids from volcanic vent systems of the Kermadec intraoceanic arc. Chem. Geol. 528, 119289.
Kleint, C., Zitoun, R., Neuholz, R., Walter, M., Schnetger, B., Klose, L., Chiswell, S.M., Middag, R., Laan, P., Sander, S.G., Koschinsky, A., 2022. Trace metal dynamics in shallow hydrothermal plumes at the Kermadec arc. Front. Mar. Sci. 8, 782734.
Metz, S., Trefry, J.H., 2000. Chemical and mineralogical influences on concentrations of trace metals in hydrothermal fluids. Geochim. Cosmochim. Acta 64 (13), 2267–2279.
Milletto, M., Wang, X., Planavsky, N.J., Luther, G.W., Lyons, T.W., Tebo, B.M., 2021. Marine microbial Mn(II) oxidation mediates Cr(III) oxidation and isotope fractionation. Geochim. Cosmochim. Acta 297, 101–119.
Mingot, A., Claustre, H., Uitz, J., Poteau, A., D'Ortenzio, F., Xing, X., 2014. Understanding the seasonal dynamics of phytoplankton biomass and the deep chlorophyll maximum in oligotrophic environments: A Bio-Argo float investigation. Glob. Biogeochem. Cy. 28 (8), 856–876.
Moos, S.B., Boyle, E.A., 2019. Determination of accurate and precise chromium isotope ratios in seawater samples by MC-ICP-MS illustrated by analysis of SAFe Station in the North Pacific Ocean. Chem. Geol. 511, 481–493.
Moos, S.B., Boyle, E.A., Altabet, M.A., Bourbonnais, A., 2020. Investigating the cycling of chromium in the oxygen deficient waters of the Eastern Tropical North Pacific Ocean and the Santa Barbara Basin using stable isotopes. Mar. Chem. 221, 103756.
Murray, J.W., Spell, B., Paul, B., 1983. The contrasting geochemistry of manganese and chromium in the eastern tropical Pacific Ocean. In: Wong C.S., Boyle E., Bruland K.W., Burton J.D., Goldberg E.D. (eds) Trace Metals in Sea Water. NATO Conference Series (IV Marine Sciences), 9. Springer, Boston, MA, pp. 643–669.
Nasemann, P., Janssen, D.J., Rickli, J., Grasse, P., Franck, M., Jaccard, S.L., 2020. Chromium reduction and associated stable isotope fractionation restricted to anoxic shelf waters in the Peruvian Oxygen Minimum Zone. Geochim. Cosmochim. Acta 285, 207–224.
Neuholz, R., Kleint, C., Schnetger, B., Koschinsky, A., Laan, P., Middag, R., Sander, S., Thal, J., Türke, A., Walter, M., Zitoun, R., 2020. Submarine hydrothermal discharge and fluxes of dissolved Fe and Mn, and He isotopes at brothers volcano based on radium isotopes. Minerals 10 (11), 969.
Orsi, A.H., Whitworth III, T., Nowlin Jr, W.D., 1995. On the meridional extent and fronts of the Antarctic Circumpolar Current. Deep Sea Res. I 42, 641–673.
Pettine, M., Millero, F.J., La Noce, T., 1991. Chromium (III) interactions in seawater through its oxidation kinetics. Mar. Chem. 34 (1–2), 29–46.
Pettine, M., D'Ottone, L., Campanella, L., Millero, F.J., Passino, R., 1998. The reduction of chromium (VI) by iron (II) in aqueous solutions. Geochim. Cosmochim. Acta 62 (9), 1509–1519.
Planavsky, N.J., Reinhard, C.T., Wang, X., Thomson, D., McGoldrick, P., Rainbird, R. H., Johnson, T., Fischer, W.W., Lyons, T.W., 2014. Low Mid-Proterozoic atmospheric oxygen levels and the delayed rise of animals. Science 346 (6209), 635–638.
Pöppelmeier, F., Janssen, D.J., Jaccard, S.L., Stocker, T.F., 2021. Modeling the marine chromium cycle: New constraints on global-scale processes. Biogeosciences 18, 5447–5463.
Reinhard, C.T., Planavsky, N.J., Robbins, L.J., Partin, C.A., Gill, B.C., Lalonde, S.V., Bekker, A., Konhauser, K.O., Lyons, T.W., 2013. Proterozoic ocean redox and biogeochemical stasis. Proc. Nat. Acad. Sci. USA 110 (14), 5357–5362.
Remmelzwaal, S.R.C., Sadekov, A.Y., Parkinson, I.J., Schmidt, D.N., Titelboim, D., Abramovich, S., Roepert, A., Kienhuis, M., Polerecky, L., Goring-HArford, H., et al., 2019. Post-depositional overprinting of chromium in foraminifera. Earth Planet Sci. Let. 515, 100–111.
Resing, J.A., Sedwick, P.N., German, C.R., Jenkins, W.J., Moffett, J.W., Sohst, B.M., Tagliabue, A., 2015. Basin-scale transport of hydrothermal dissolved metals across the South Pacific Ocean. Nature 523 (7559), 200–203.
Rickli, J., Janssen, D.J., Hassler, C., Ellwood, M.J., Jaccard, S.L., 2019. Chromium biogeochemistry and stable isotope distribution in the Southern Ocean. Geochim. Cosmochim. Acta 262, 188–206.
Rudnick, R.L., Gao, S., 2003. 3.01 – Composition of the Continental Crust. Editor(s): H.D. Holland, K.K. Turekian. In: Treatise on Geochemistry, Pergamon, Oxford, pp. 1–64.
Rudnicki, M.D., Elderfield, H., 1993. A chemical model of the buoyant and neutrally buoyant plume above the TAG vent field, 26 degrees N, Mid-Atlantic Ridge. Geochim. Cosmochim. Acta 57 (13), 2939–2957.
Rue, E.L., Smith, G.J., Cutter, G.A., Bruland, K.W., 1997. The response of trace element redox couples to suboxic conditions in the water column. Deep Sea Res. I. 44 (1), 113–134.

Sander, S., Koschinsky, A., 2000. Onboard-ship redox speciation of chromium in diffuse hydrothermal fluids from the North Fiji Basin. Mar. Chem. 71 (1–2), 83–102.
Sander, S., Koschinsky, A., 2011. Metal flux from hydrothermal vents increased by organic complexation. Nat. Geosci. 4, 145–150.
Scheiderich, K., Amini, M., Holmden, C., Francois, R., 2015. Global variability of chromium isotopes in seawater demonstrated by Pacific, Atlantic, and Arctic Ocean samples. Earth Planet. Sci. Lett. 423, 87–97.
Schoenberg, R., Zink, S., Staubwasser, M., von Blanckenburg, F., 2008. The stable Cr isotope inventory of solid Earth reservoirs determined by double spike MC-ICP-MS. Chem. Geol. 249, 294–306.
Semeniuk, D.M., Maldonado, M.T., Jaccard, S.L., 2016. Chromium uptake and adsorption in marine phytoplankton – Implications for the marine chromium cycle. Geochim. Cosmochim. Acta 184, 41–54.
Sloyan, B.M., Rintoul, S.R., 2001. The Southern Ocean Limb of the Global Deep Overturning Circulation. J Phys. Oc. 31 (1), 143–173.
Sokolov, S., Rintoul, S., 2000. Circulation and water masses of the southwest Pacific: WOCE Section P11, Papua New Guinea to Tasmania. J. Mar. Res. 58 (2), 223–268.
Tréguer, P.J., de la Rocha, C.L., 2013. The World Ocean Silica Cycle. An. Rev. Mar. Sci. 5, 477–501.
Trocine, R.P., Trefry, J.H., 1988. Distribution and chemistry of suspended particles from an active hydrothermal vent site on the Mid-Atlantic Ridge at 26°N. Earth Planet. Sci. Let. 88 (1–2), 1–15.
Wang, X., 2021. The chromium isotope fractionation factor in seawater. Chem. Geol. 579, 120358.
Wang, W.X., Griscom, S.B., Fisher, N.S., 1997. Bioavailability of Cr(III) and Cr(VI) to Marine Mussels from Solute and Particulate Pathways. Environ. Sci. Tech. 31 (2), 603–611.
Wang, C., Reinhard, C.T., Rybacki, K.S., Hardisty, D.S., Ossa, F.O., Wang, X., Hofmann, A., Asael, D., Robbins, L.J., Zhang, L., Planavsky, N.J., 2021. Chromium isotope systematics and the diagenesis of marine carbonates. Earth Planet. Sci. Let. 562, 116824.
Wanner, C., Sonnenthal, E.L., 2013. Assessing the control on the effective kinetic Cr isotope fractionation factor: A reactive transport modeling approach. Chem. Geol. 337–338, 88–98.
Wei, W., Frei, R., Chen, T., Klaebe, R., Wei, G., Li, D., Ling, H., 2018. Marine ferromanganese oxide: a potentially important sink of light chromium isotopes? Chem. Geol. 495, 90–103.
Xia, J., Qin, L., Shen, J., Carlson, R.W., Ionov, D.A., Mock, T.D., 2017. Chromium isotope heterogeneity in the mantle. Earth Planet. Sci. Let. 464, 103–115.
Yamakawa, A., Yamashita, K., Makishima, A., Nakamura, E., 2009. Chemical separation and mass spectrometry of Cr, Fe, Ni, Zn, and Cu in Terrestrial and extraterrestrial materials using thermal ionization mass spectrometry. Anal. Chem. 81 (23), 9787–9794.
Yobo, L.N., Holmden, C., Brandon, A.D., Lau, K.V., Eldrett, J.S., Bergman, S., 2022. LIP volcanism (not anoxia) tracked by Cr isotopes during Ocean Anoxic Event 2 in the proto-North Atlantic region. Geochim. Cosmochim. Acta.
Zilberman, N.V., Roemmich, D.H., Gilson, J., 2020. Deep-ocean circulation in the Southwest Pacific Ocean interior: Estimates of the mean flow and variability using Deep Argo data. Geophys. Res. Lett. 47 (13). e2020GL088342.
Zink, S., Schoenberg, R., Staubwasser, M., 2010. Isotopic fractionation and reaction kinetics between Cr(III) and Cr(VI) in aqueous media. Geochim. Cosmochim. Acta 74 (20).